1-1-2002

Net planes in decagonal Al-Ni-Co

Jennifer Kay Bjergaard
Iowa State University

Net planes in decagonal Al-Ni-Co

by

Jennifer Kay Bjergaard

A thesis submitted to the graduate faculty

in partial fulfillment of the requirements for the degree of

MASTER OF SCIENCE

Major: Analytical Chemistry

Program of Study Committee:
Patricia A. Thiel (Major Professor)
Mei Hong
Daniel J. Sordelet

Iowa State University

Ames, Iowa

2002

Graduate College
Iowa State University

This is to certify that the master's thesis of

Jennifer Kay Bjergaard

has met the thesis requirements of Iowa State University

Signatures have been redacted for privacy

DEDICATION

To my parents

For their love and support

TABLE OF CONTENTS

INTRODUCTION

Workers at the National Bureau of Standards discovered the presence quasicrystals in 1982, and published their results in 1984, after an Al-Mn alloy produced 10-fold, 2-fold and 3-fold diffraction patterns, indicating that the sample had 5-fold symmetry.[1] This result surprised scientists, since 5-fold symmetry went against conventional crystal concepts.[2] Prior to the discovery of quasicrystals, crystals were viewed as well-ordered arrangements of atoms or molecules within a latticework composed of identical "unit cells." The unit cells were considered to be the building blocks, each containing the same distribution of atoms, which fit together regularly and periodically to fill space.[3] Thus, it was inherent in every crystal structure that only certain symmetries could exist: the 2, 3, 4, and 6-fold symmetries. A crystal could not possibly have 5-fold symmetry. Having 5-fold symmetry in crystals would be like trying to tile a floor using only pentagonal tiles. It would not be possible to cover the floor completely without overlap. Similarly, it is impossible to pack shapes that have 5-fold symmetry in three dimensions without some degree of frustration or overlap.[2] Quasicrystals overcome this apparent contradiction, however, by consisting of atoms aperiodically arranged to achieve long-range order.

Since their discovery, many different quasicrystals have been produced. Quasicrystals can be structurally divided into three classifications: three-dimensional, two-dimensional, and one-dimensional quasicrystals. The three-dimensional classification contains quasicrystals with aperiodic spacing in three directions. The only known materials in this group are the icosahedral quasicrystals,

which are 5-fold symmetric. The two-dimensional classification includes octagonal (8-fold symmetry), decagonal (10-fold symmetry), and dodecagonal (12-fold symmetry) quasicrystals. These quasicrystals are aperiodic in two directions while being periodic in the third direction. Finally, the one-dimensional classification is periodic in two directions and quasiperiodic in one direction. Ebert et al have previously discussed one-dimensional quasicrystals.[4] The work presented here focuses on the decagonal quasicrystal Al-Ni-Co.

The conventional viewpoint of decagonal quasicrystals is that they are geometrically composed of aperiodic planes stacked periodically, with no coupling between the aperiodic and periodic axes. However, when examining the relationship between the 10-fold and 2-fold axes in decagonal Al-Ni-Co during its growth morphology, Tsai et al discovered facets inclining towards the 10-fold axis (see Figure 1).[5] These facets indicate that there are stable planes relating the periodic and aperiodic directions. These planes may play a role in establishing aperiodic long-range order in the quasicrystal. Steurer calls these planes "net planes."[6]

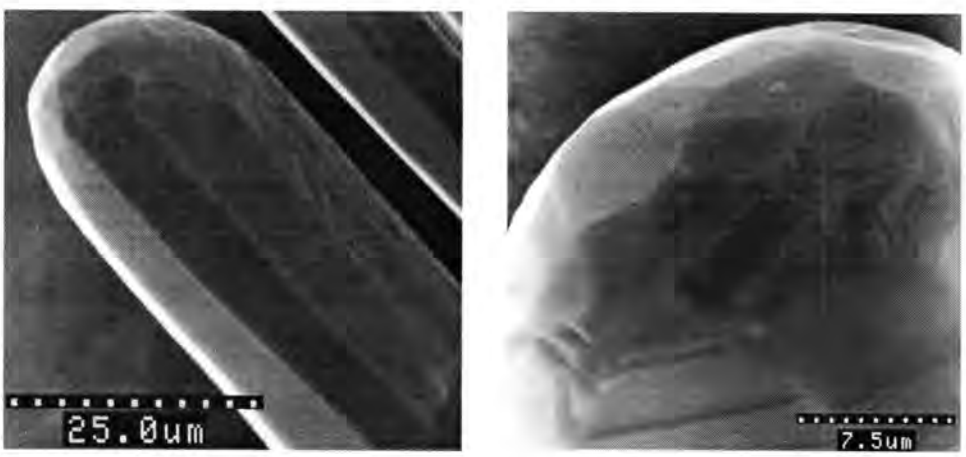

Figure 1: Growth morphology of decagonal Al-Ni-Co.[6] *(used with permission)*

Conceptually, net planes are comparable to lattice planes for periodic crystals. Periodic crystal structures can be broken down into an infinite number of geometrical points called lattices. Within the lattice, every point has identical surroundings and all the lattice points are equivalent. The identical points of a lattice can be arranged periodically in three-dimensional space in only 14 arrangements, called Bravais lattices.[7] There are an infinite number of parallel lattice planes associated with any Bravais lattice, each distinguished by its point arrangement (hkl) and by its specific interplanar spacing (d_{hkl}). Each set of lattice planes is stacked so that all the atoms in the structure are included.[3] Additionally, these structures exhibit translational symmetry. Thus, it is possible to translate, or move, one part of the crystal so that it matches up precisely with another part of the crystal. Consequently, by examining any small part of the crystal, the exact position and spacing in any other part can be determined.[2]

In contrast, quasicrystals are not periodic and therefore do not contain a lattice. As a result, quasicrystals lack lattice planes and do not exhibit translational symmetry. However, quasicrystals do contain aperiodic stacks of atomic layers. In Al-Ni-Co, the periodic stacking of the aperiodic atomic layers along the 10-fold axis forms one set of net planes. Technically, these planes can be called lattice planes since they are stacked periodically. Additionally, there are five symmetrically equivalent stacks of net planes perpendicular to the aperiodic plane. As previously mentioned, there are also aperiodically spaced planes inclined towards the 10-fold axis. Technically, these inclined planes are not net planes because they are non-equivalent and because aperiodically spaced planes cannot cut the 10-fold axis

periodically. Thus, they are not inclusive of all the atoms in the structure. Net planes have to be spaced periodically in order to be inclusive. To achieve periodicity, Steurer states that it is necessary to allow for a small amount of corrugation. This is accomplished using the periodic average structure of quasicrystals.[8] Appendix 1 contains further discussion of the periodic average structure of quasicrystals.

The work described in this thesis was designed to test the predictions about the existence of stable net planes. This work focused on the $(1,1,\bar{1},\bar{1},2)$ plane and the $(0,\bar{1},\bar{1},0,1)$ plane. Net planes are projected to be stable terminations of the decagonal structure; therefore, faceting of vicinal surfaces to net planes would be expected. This supposition was examined by cutting the $(1,1,\bar{1},\bar{1},2)$ plane on the predicted plane and three degrees off that plane in two different directions. Thus, if a stable net plane did exist in the $(1,1,\bar{1},\bar{1},2)$ plane, the cuts would produce identical low energy electron diffraction (LEED) patterns. In addition, stable net planes should produce LEED patterns and terrace-step structures that reflect the bulk structure. This assumption was examined for the $(0,\bar{1},\bar{1},0,1)$ plane by comparing experimental LEED patterns and scanning tunneling microscopy (STM) images to predicted LEED patterns and step heights.

EXPERIMENTAL DESCRIPTION

All experiments were performed in one of two stainless steel ultrahigh vacuum (UHV) chambers. To differentiate between the two chambers, they will be referred to as "the LEED chamber" and "the VT-STM chamber."

The LEED Chamber

Experiments in the LEED chamber operated at a typical base pressure of 2×10^{-10} Torr. The chamber consists of a differentially-pumped ion gun for sample cleaning, a single-pass cylindrical mirror analyzer (CMA) for Auger electron spectroscopy (AES), and a low energy electron diffraction (LEED) optics system. AES is used to detect impurities on the surface of the sample. LEED is typically used to determine the structure of a crystal surface. Crystals are mounted onto a coldfinger, which allows the samples to be cooled to 77 K and to be resistively heated to temperatures greater than 1000 K.

The Samples

The Al-Ni-Co samples used in the LEED chamber were cut from a boule grown at the Ames Laboratory Materials Preparation Center. For reasons mentioned previously on page four of the introduction, the first sample, ARR-2-102-2, was cut three degrees off the $(1,1,\bar{1},\bar{1},2)$ plane in the $[0,\bar{1},\bar{1},0,1]$ direction. The second sample, ARR-2-137-1, was cut parallel to the $(1,1,\bar{1},\bar{1},2)$ plane. The final sample, ARR-2-137-2, was cut three degrees off the $(1,1,\bar{1},\bar{1},2)$ plane towards the $[1,0,0,\bar{1},1]$ direction. In order to orient the samples to the $(1,1,\bar{1},\bar{1},2)$ face, Laue

patterns were utilized. For a complete description of how the Laue patterns were used to orient the samples, refer to Appendix 2.

Cleaning

After being cut, the samples were polished to a mirror finish using 6 μm, 1 μm and then 0.25 μm diamond paste. The samples were subsequently cleaned by sonication in acetone for 15 minutes followed by 15 minutes of sonication in methanol. The samples were then mounted onto a tantalum plate. Next, the tantalum plate was spot-welded to two tantalum rods, which were attached to the coldfinger. The two tantalum rods allowed the sample to be heated resistively. The sample temperature was measured with a W-5% Re vs. W-26% Re thermocouple spot-welded to the back of the tantalum plate.

After being placed in UHV, the samples were cleaned using sputter and anneal cycles. Carbon and oxygen were the major surface contaminants. In AES, carbon produces a peak at 272 eV, while oxygen produces a peak at 503 eV. The disappearance of these peaks was monitored by AES during the cleaning procedure. The samples were sputtered at a beam voltage of 1.0 kV with argon (99.99%), which was used as received from Matheson Gas Products, Inc. The samples were sputtered for 30 minutes before annealing. The samples were annealed at 400 K for 30 minutes. Subsequent anneals increased in temperature increments of 100 K and continued to last for 30 minutes. When the annealing temperature reached 900 K, the annealing time was increased to one hour. Subsequent anneals after 900 K increased by 50 K increments, each with an annealing time of one hour. When the final annealing temperature of 1100 K was

obtained, the samples were annealed for three to four hours. AES was employed during the cleaning process to ensure a clean surface. After achieving a clean sample surface, the samples were sputtered with argon for 30 minutes and annealed at 1100 K for two to four hours before performing the LEED experiments.

LEED

Once a clean surface was obtained, LEED patterns were recorded using a VCR. The VCR was coupled to a Page-MIT SIT 66 video camera, which was focused on the LEED optics screen. Beam energy increments were synchronized with the time display on the VCR while the tape was recording. LEED images were then captured from the VCR tape to the computer using the computer program NIH-Image, which is available at http://rsb.info.nih.gov/nih-image/.

The VT-STM Chamber

Experiments in the VT-STM chamber operated at a typical base pressure of 2×10^{-10} Torr. The chamber consists of an ion gun for sample cleaning, a combined retarding field analyzer for AES and LEED optics system, and an Omicron variable temperature scanning tunneling microscope (VT-STM). The VT-STM is used to determine the surface structure of a sample.

The Sample

The Al-Ni-Co sample used in the VT-STM chamber was cut from a boule grown at the Ames Laboratory Materials Preparation Center. The sample was cut to the $(0,\bar{1},\bar{1},0,1)$ plane, using the orientation recommended by Steurer after x-raying the sample.

Cleaning

After being cut, the samples were prepared in the same manner as for the LEED chamber. The sample was then mounted onto a special tantalum plate and inserted into the chamber. The sample was heated radiatively using a tungsten filament. Sample temperature was measured with a chromel-alumel thermocouple mounted on the manipulator near the sample plate. This thermocouple had been previously calibrated to correct for temperature differences between the sample plate and the contact point of the thermocouple on the manipulator.

Once in UHV, the samples were cleaned using the same procedure as in the LEED chamber. However, in the VT-STM chamber, the samples were sputtered with argon at a beam voltage of 2.0 kV using a sputtering angle of 45°. By sputtering at 45°, it was hoped that larger terraces would result in the STM images. Also, the final annealing temperature was changed to 1075 K.

LEED

Once a clean surface on the sample was obtained, LEED patterns were captured via a digital camera coupled to a computer. The digital camera was focused on the LEED optics screen. When the desired beam energy was set using the LEED optics controls, the image was captured using the Multi-LEED computer program.

VT-STM

After a clean surface was obtained, the sample was transferred to the VT-STM portion of the chamber. Although the VT-STM is able to conduct scans at various sample temperatures, only room temperature scans were performed.

Imaging was performed in constant current mode using a sample bias of ± 1.0 V and a tunneling current between 0.3 nA and 0.5 nA. Images were scanned using an electrochemically etched tungsten tip. STM images were recorded using the Scala Pro 3.1 program. The STM images ranged over a wide scale, from 1000 x 1000 nm^2 to 10 x 10 nm^2.

RESULTS AND DISCUSSION

The LEED Chamber

All LEED patterns obtained from the three samples oriented around the $(1,1,\bar{1},\bar{1},2)$ plane were not very intense (See Figure 2). In addition, the patterns diminished in intensity with time. After approximately 30 minutes, the LEED pattern virtually disappeared. Therefore, the samples were extremely sensitive to surface contamination. In contrast, LEED patterns of Al-Ni-Co oriented to the 10-fold axis are known to be quite stable, easily lasting over one day.

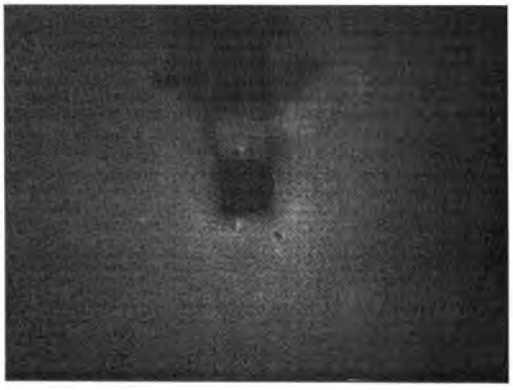

60 eV

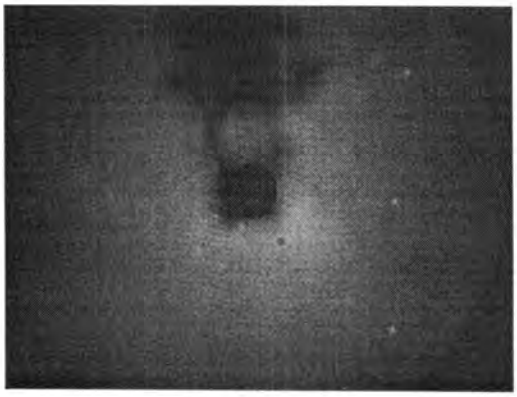

70 eV

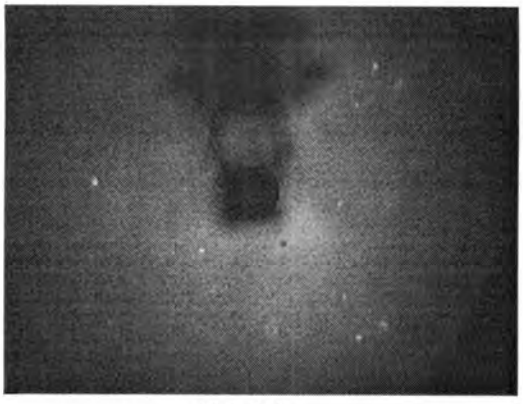

80 eV

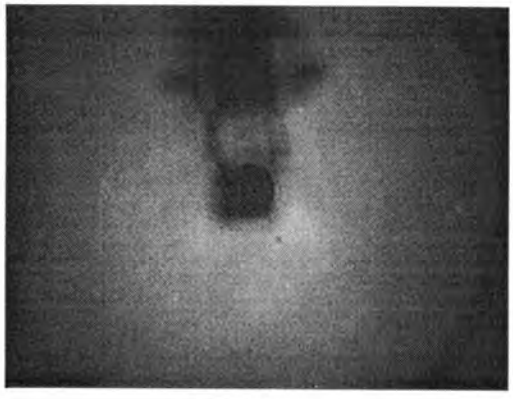

90 eV

Figure 2: LEED patterns obtained from Al-Ni-Co oriented to the $(1,1,\bar{1},\bar{1},2)$ plane.

In order to clearly see the LEED spots in the images pictured in Figure 2, the spots were enhanced to equal intensities using the Adobe Photoshop computer program, which is available at http://www.adobe.com/products/photoshop/main.html (See Figure 3). Closer examination of the LEED patterns shown in Figure 3 revealed that the spots moved towards the center of the image with increasing beam energy. Thus, if faceting did occur, it was not far off of the surface normal.

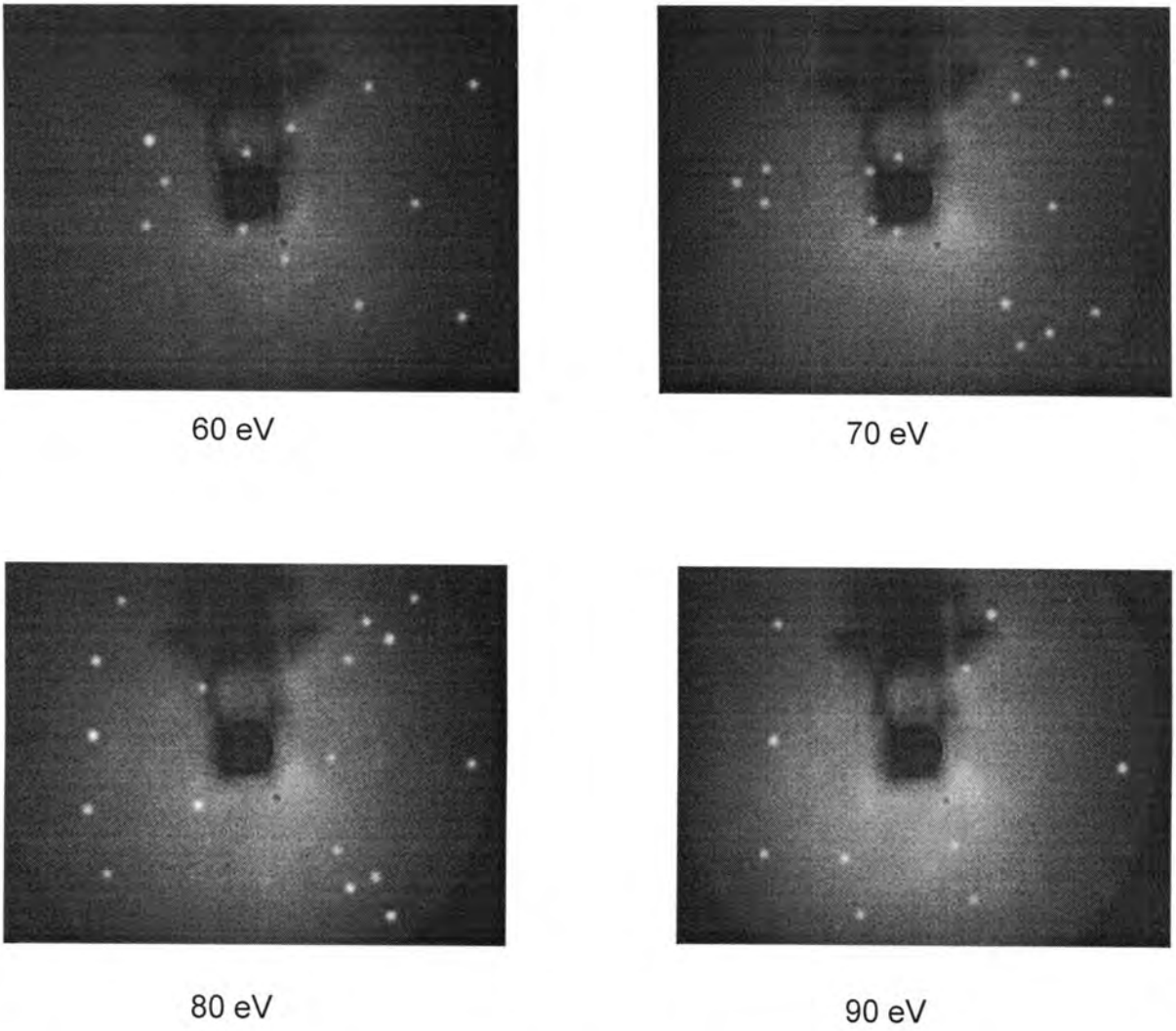

Figure 3: Enhanced LEED patterns obtained from Al-Ni-Co oriented to the $(1,1,\bar{1},\bar{1},2)$ plane.

Examination of the enhanced LEED patterns in Figure 3 reveals that these images only have one mirror plane, running horizontally across the image. These results resemble the Laue patterns received for the samples (see Figure 4). Like the LEED patterns, the Laue patterns were of very low intensity and contained only one mirror plane in the horizontal direction. This similarity is expected since both LEED patterns and Laue patterns occur in reciprocal space.

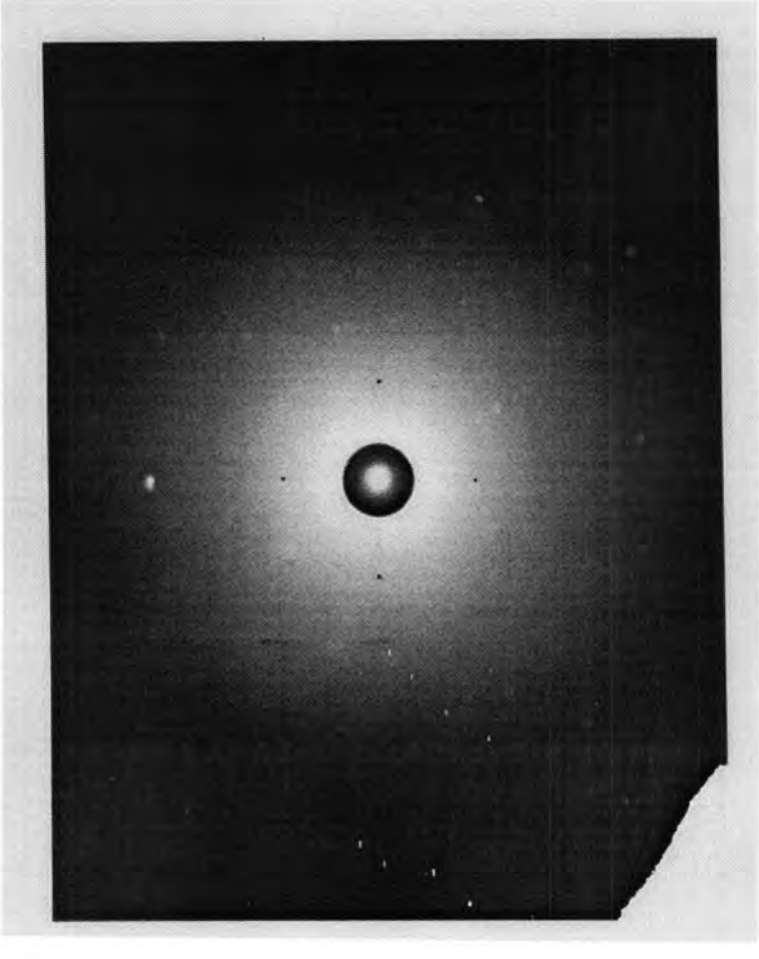

Figure 4: A Laue pattern obtained while trying to orient the decagonal Al-Ni-Co samples to the $(1,1,\bar{1},\bar{1},2)$ plane.

The LEED patterns shown in Figure 3 are quite different from LEED patterns of Al-Ni-Co oriented to the 10-fold and 2-fold axes. Both the 10-fold and 2-fold LEED patterns contain vertical and horizontal mirror planes, such as shown in the 10-fold LEED pattern in Figure 5.

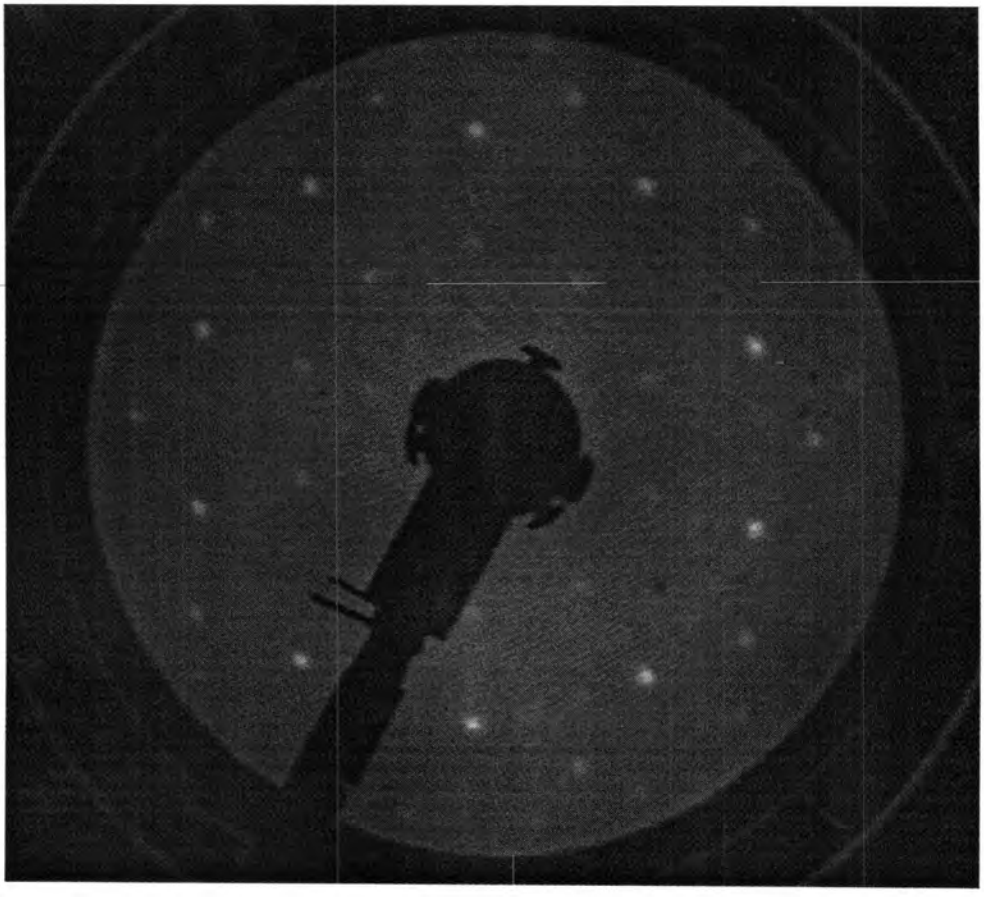

Figure 5: LEED pattern of decagonal Al-Ni-Co oriented to the 10-fold axis.

Evidence supporting the existence of inclined net planes can be found in a comparison of all LEED images obtained from the samples in the LEED chamber (see Figure 6). This comparison reveals that samples ARR-2-137-1 and ARR-2-137-2 produced identical LEED patterns. Sample ARR-2-102-2, however, produced LEED patterns that differed from those produced by the other two samples.

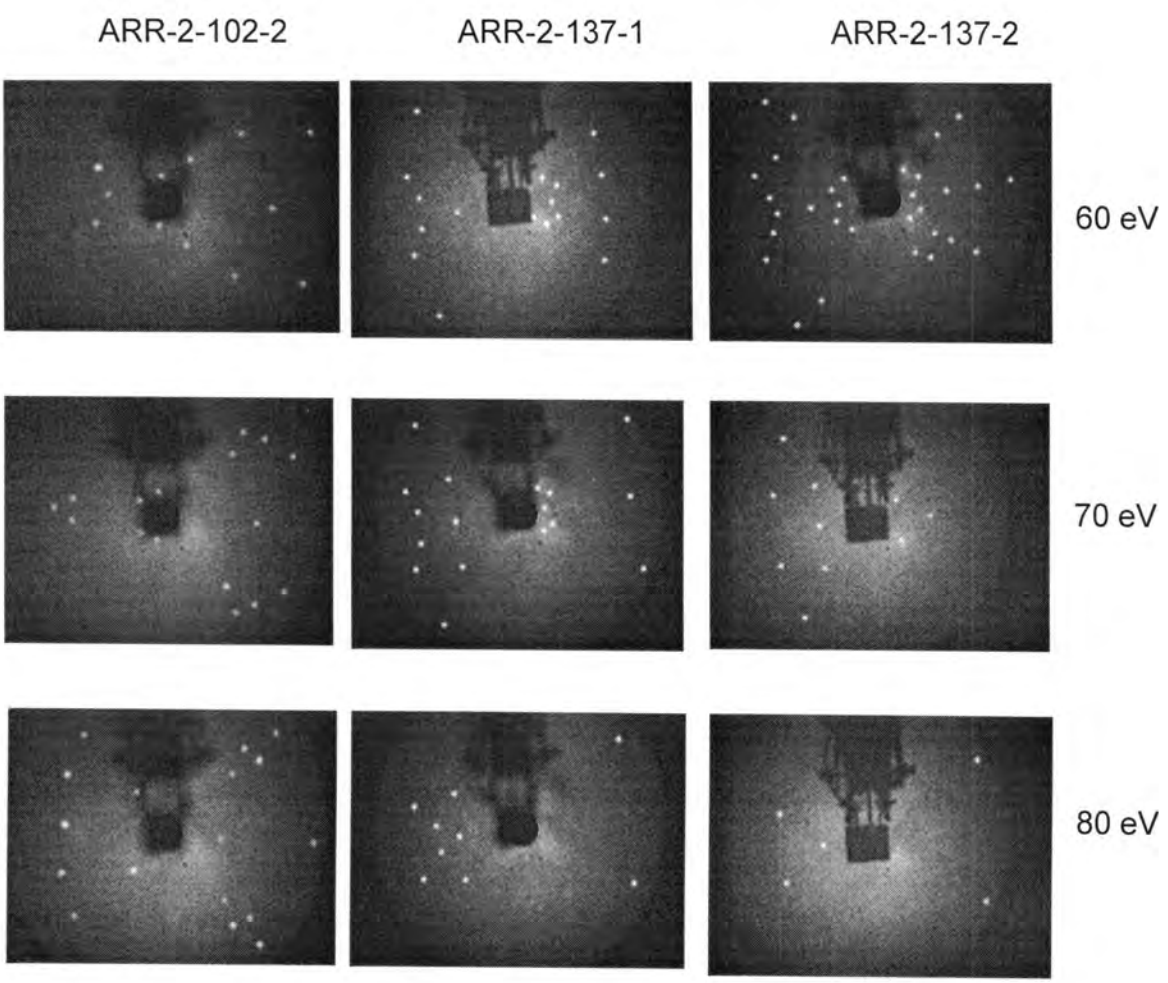

Figure 6: Comparison of LEED patterns for the three Al-Ni-Co samples oriented around the $(1,1,\bar{1},\bar{1},2)$ plane.

Since samples ARR-2-137-1 and ARR-2-137-2 produced identical LEED patterns yet are not cut along the same plane, it is evident that they are faceting to the same plane. Thus, these samples provide evidence that a stable net plane linking the 10-fold and the 2-fold axes exists. The fact that ARR-2-102-2 produced a different LEED pattern than the other two samples implies that its orientation also causes it to facet to a stable net plane, albeit a different net plane than utilized by samples ARR-2-17-1 and ARR-2-137-2. Comparison of LEED patterns from sample ARR-2-102-2 to the LEED patterns obtained from the STM chamber indicates that this sample faceted to the $(0,\bar{1},\bar{1},0,1)$ plane. This result makes sense, since sample ARR-2-102-2 was oriented three degrees off the $(1,1,\bar{1},\bar{1},2)$ plane towards the $[0,\bar{1},\bar{1},0,1]$ direction.

A second type of LEED pattern was also found for all three samples in the LEED chamber. These LEED patterns consisted of lines instead of spots, as indicated in Figure 7. These lined LEED patterns tend to occur in samples that are periodic in one direction and disordered in another. For example, LEED patterns containing lines have been observed in experiments of adsorbate structures on single-crystal surfaces.[9, 10, 11] Further discussion on the lined LEED patterns can be found in Appendix 3.

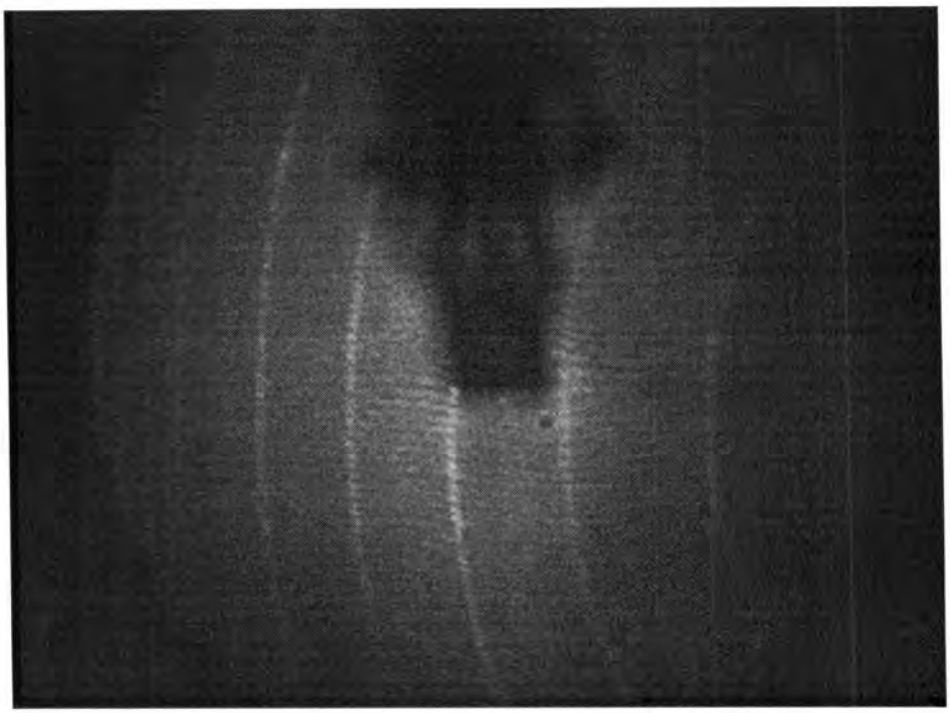

Figure 7: LEED pattern of Al-Ni-Co oriented around the $(1,1,\bar{1},\bar{1},2)$ plane containing lines, rather than spots.

The VT-STM Chamber

LEED

The LEED patterns obtained from the Al-Ni-Co sample oriented to the $(0,\bar{1},\bar{1},0,1)$ plane are shown in Figure 8. Like the LEED patterns from the samples oriented around the $(1,1,\bar{1},\bar{1},2)$ plane, the intensity of the LEED spots would diminish with time, becoming significantly less intense after approximately 30 minutes. Thus, theses samples were also highly sensitive to surface contaminants. In addition, the LEED patterns contain only one mirror plane: a plane running horizontally across the image. Unlike the previous patterns, however, the intensity of the patterns did not require enhancing.

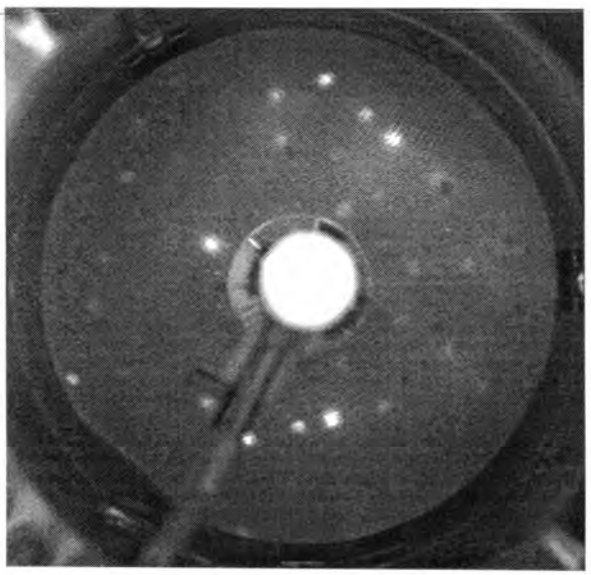

30 eV

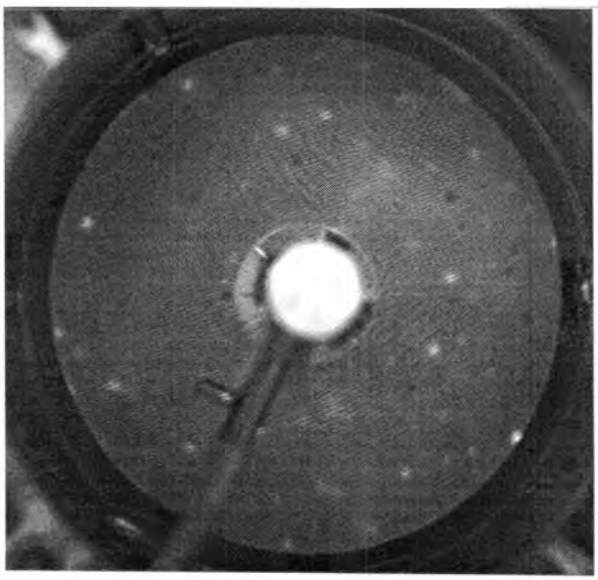

40 eV

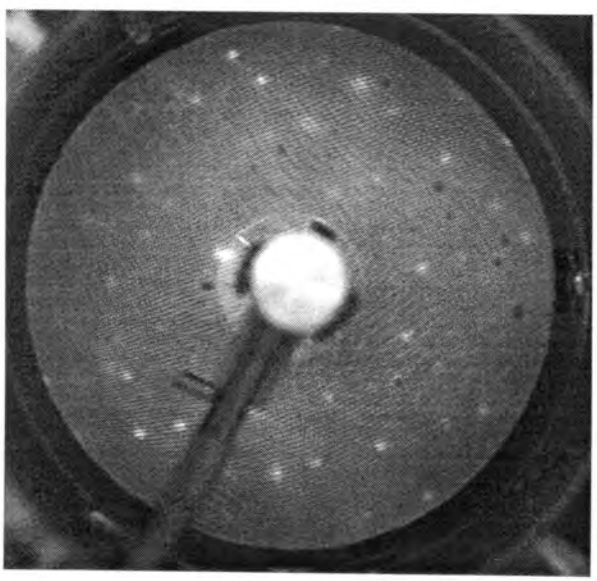

50 eV

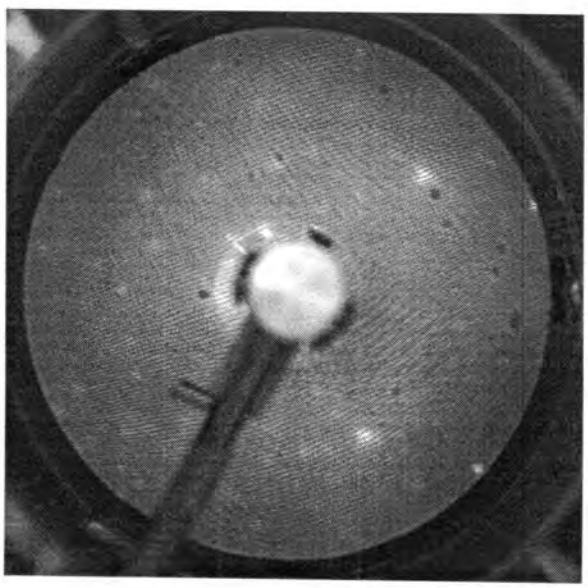

60 eV

Figure 8: LEED images from decagonal Al-Ni-Co oriented to the $(0,\bar{1},\bar{1},0,1)$ plane.

The LEED patterns obtained from the sample oriented to the $(0,\bar{1},\bar{1},0,1)$ plane were compared to LEED patterns predicted by Steurer for this particular plane (see Figure 9). For a complete description of this comparison, refer to Appendix 4 The result of the comparison was that the experimental LEED patterns obtained for the Al-Ni-Co sample did not adequately match the LEED patterns predicted by Steurer. Therefore, it was concluded that the LEED patterns shown in Figures 8 and 9 were not the same.

As with the $(1,1,\bar{1},\bar{1},2)$ surfaces, LEED images containing lines instead of spots could be obtained for the sample oriented to the $(0,\bar{1},\bar{1},0,1)$ plane. An example of this type of LEED pattern is shown in Figure 10. These lined LEED patterns are discussed further in Appendix 3.

Finally, the Al-Ni-Co sample in the VT-STM chamber also provided evidence for the existence of net planes. As mentioned previously, sample ARR-2-102-2 from the LEED chamber, which was cut three degrees off of the $(1,1,\bar{1},\bar{1},2)$ plane in the $[0,\bar{1},\bar{1},0,1]$ direction, appeared to facet to the $(0,\bar{1},\bar{1},0,1)$ plane. This faceting can be verified in Figure 11. Here, the LEED patterns obtained for sample ARR-2-102-2 are compared to those acquired for the sample in the VT-STM chamber. It is apparent that the LEED patterns for the two different orientations are producing the same LEED pattern. Thus, the two samples are faceting to the same plane.

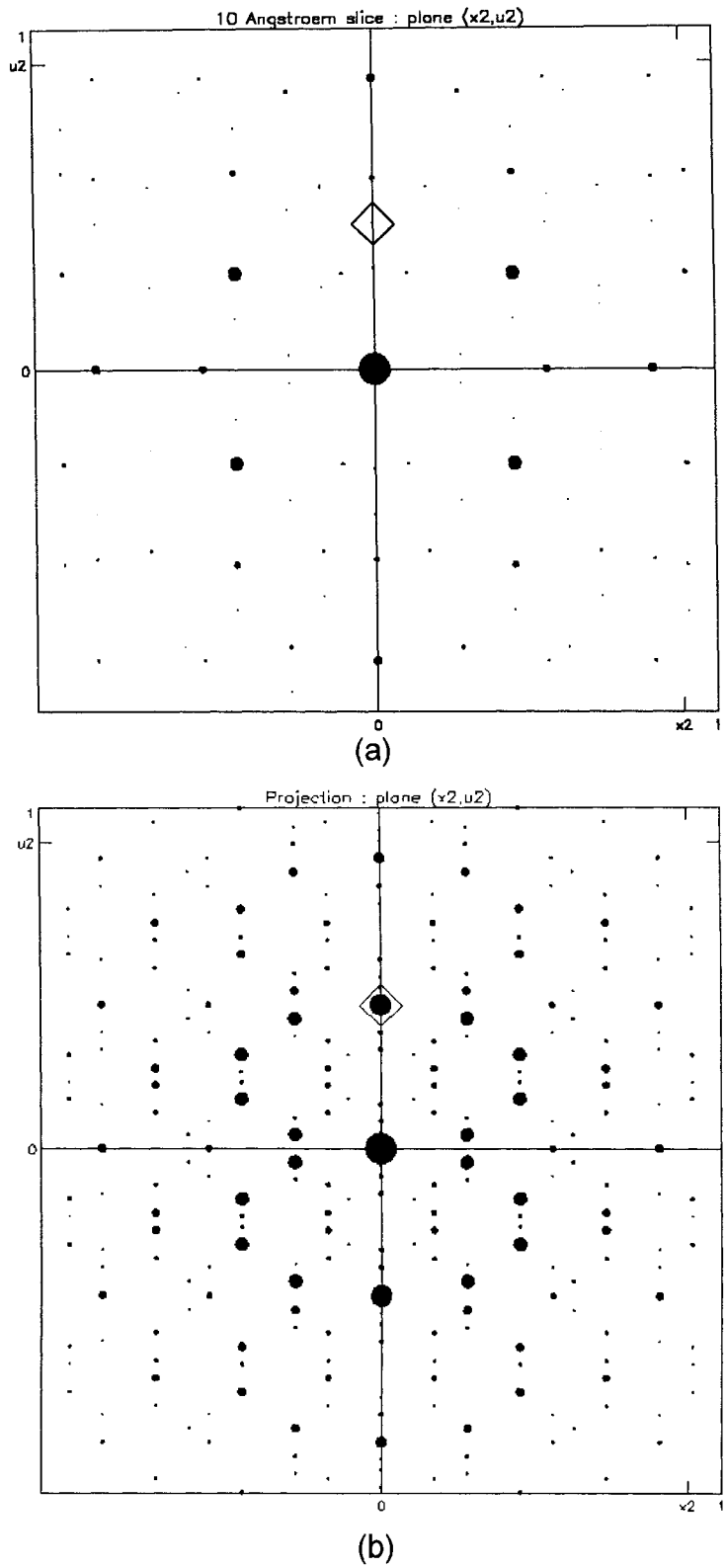

Figure 9: Predicted LEED patterns for decagonal Al-Ni-Co oriented to the $(0,\bar{1},\bar{1},0,1)$ plane. (a) assumes a 1 nm penetration depth for the radiation , while (b) is for an infinitely thin net plan.

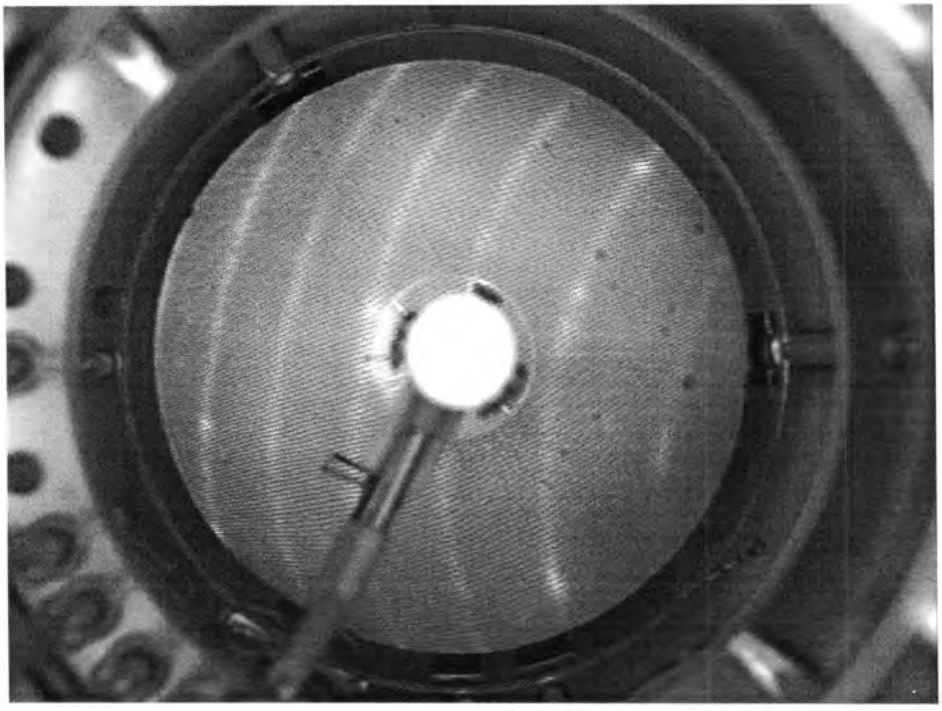

Figure 10: LEED pattern of Al-Ni-Co oriented to the $(0,\bar{1},\bar{1},0,1)$ plane showing lines rather than spots.

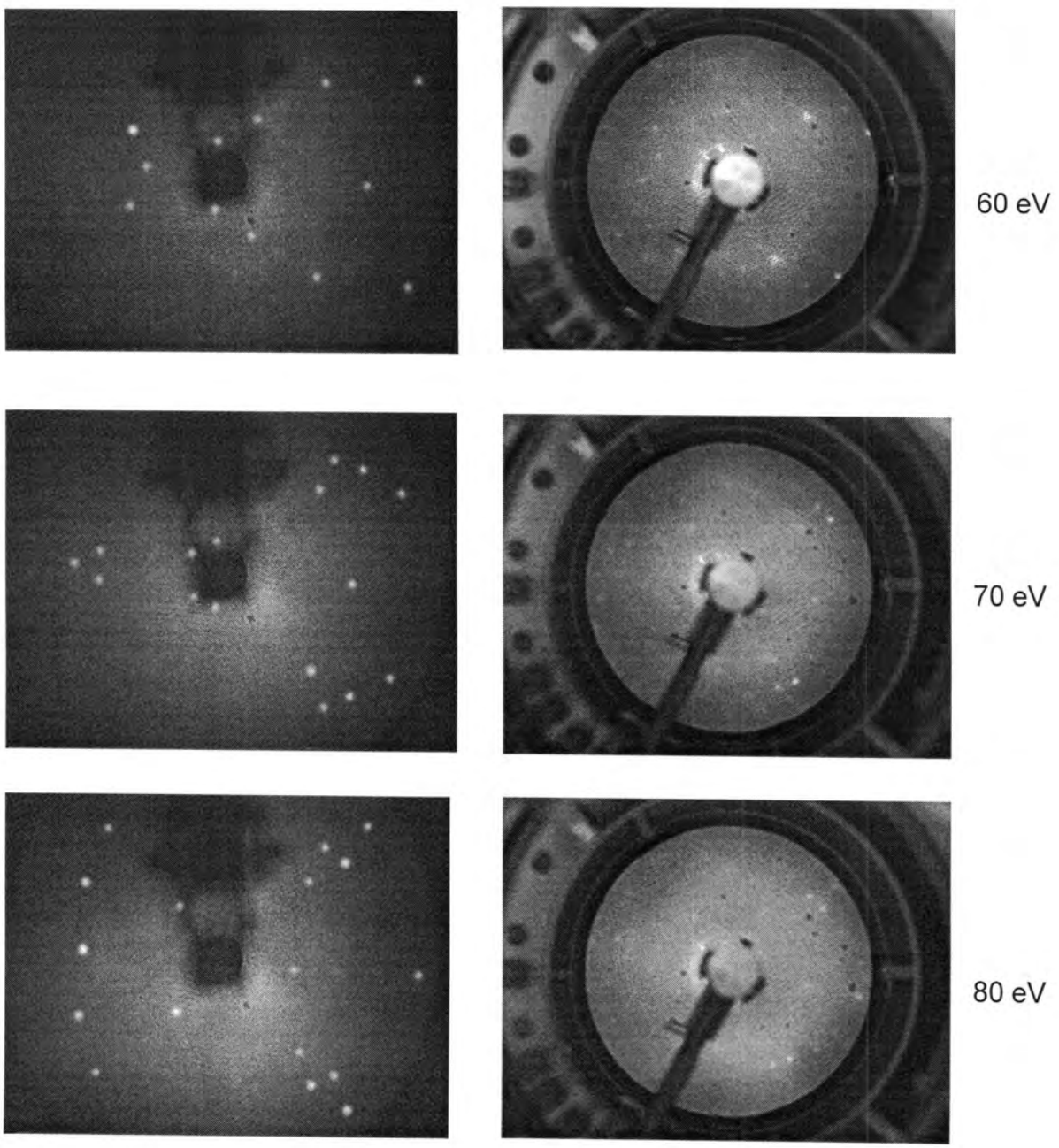

Figure 11: Comparison of sample ARR-2-102-2, which was cut three degrees off of the $(1,1,\bar{1},\bar{1},2)$ plane, to the sample oriented to the $(0,\bar{1},\bar{1},0,1)$ plane at various beam energies.

VT-STM

The STM images obtained ranged from a scale of 1000 x 1000 nm^2 to 10 x 10 nm^2. The images obtained are shown below in Figures 12-18.

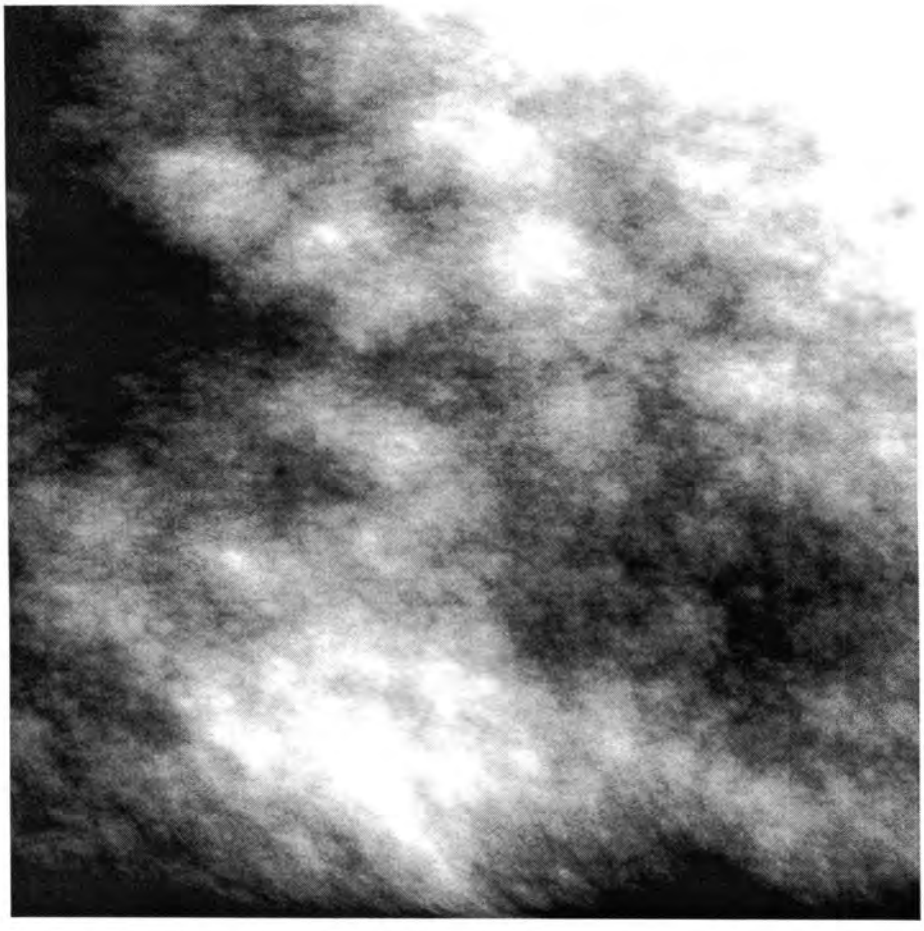

1000 x 1000 nm^2

Figure12: STM image obtained from Al-Ni-Co oriented to the $(0,\bar{1},\bar{1},0,1)$ plane.

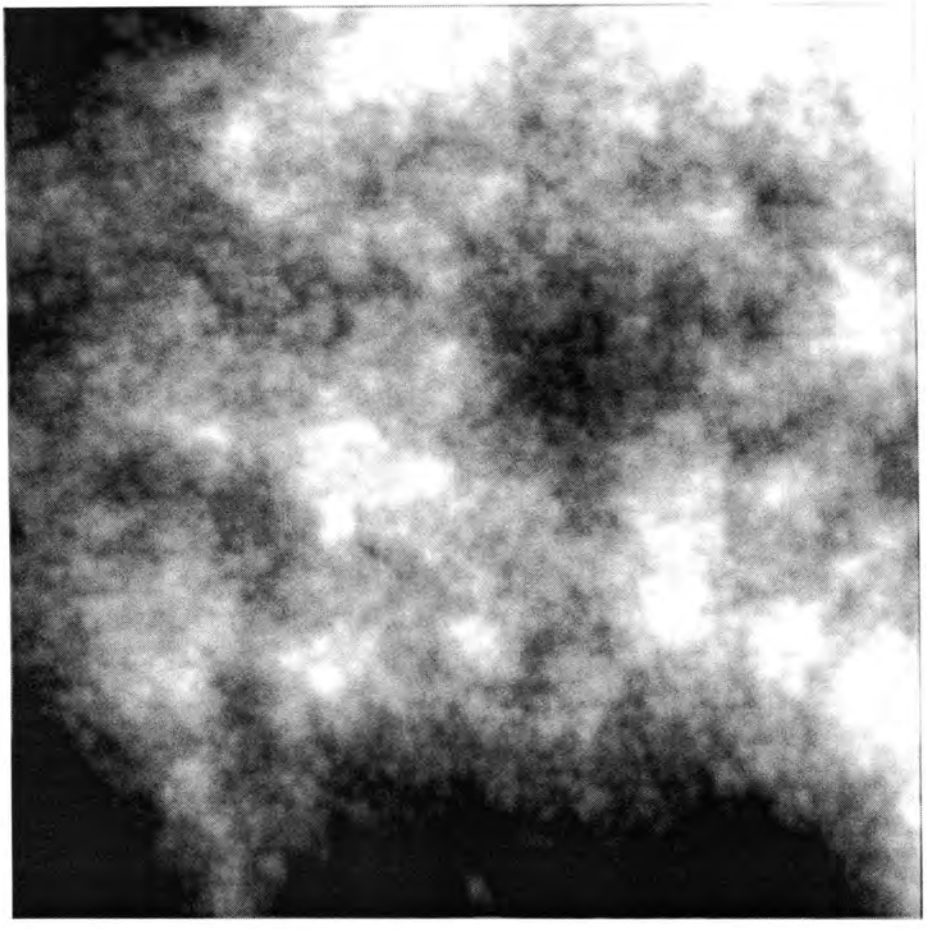

500 x 500 nm^2

Figure 13: STM image obtained from Al-Ni-Co oriented to the $(0,\bar{1},\bar{1},0,1)$ plane.

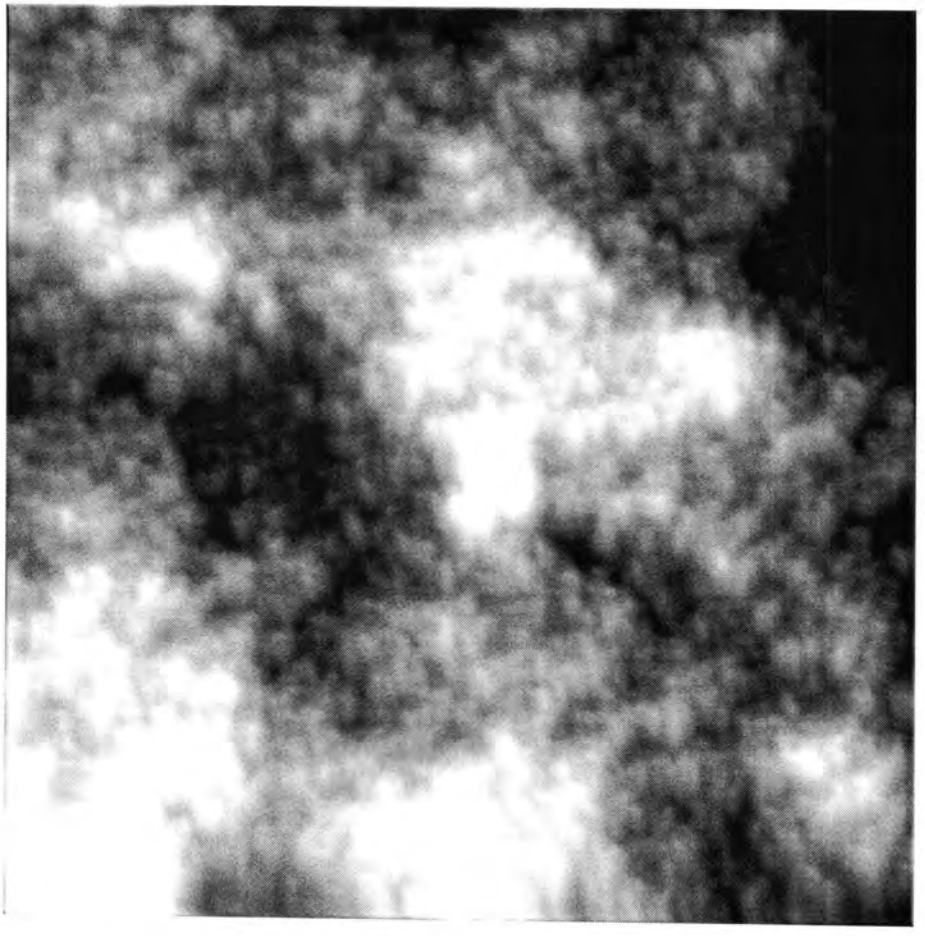

250 x 250 nm^2

Figure 14: STM image obtained from Al-Ni-Co oriented to the $(0,\bar{1},\bar{1},0,1)$ plane.

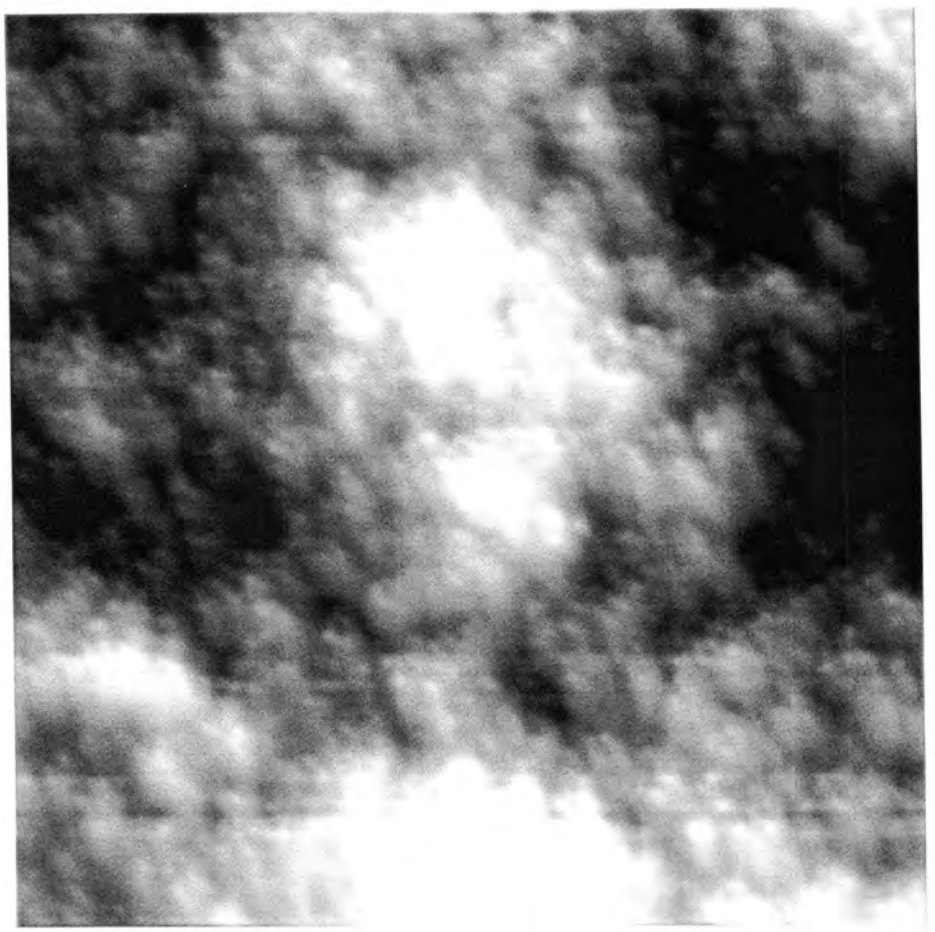

100 x 100 nm^2

Figure 15: STM image obtained from Al-Ni-Co oriented to the $(0,\bar{1},\bar{1},0,1)$ plane.

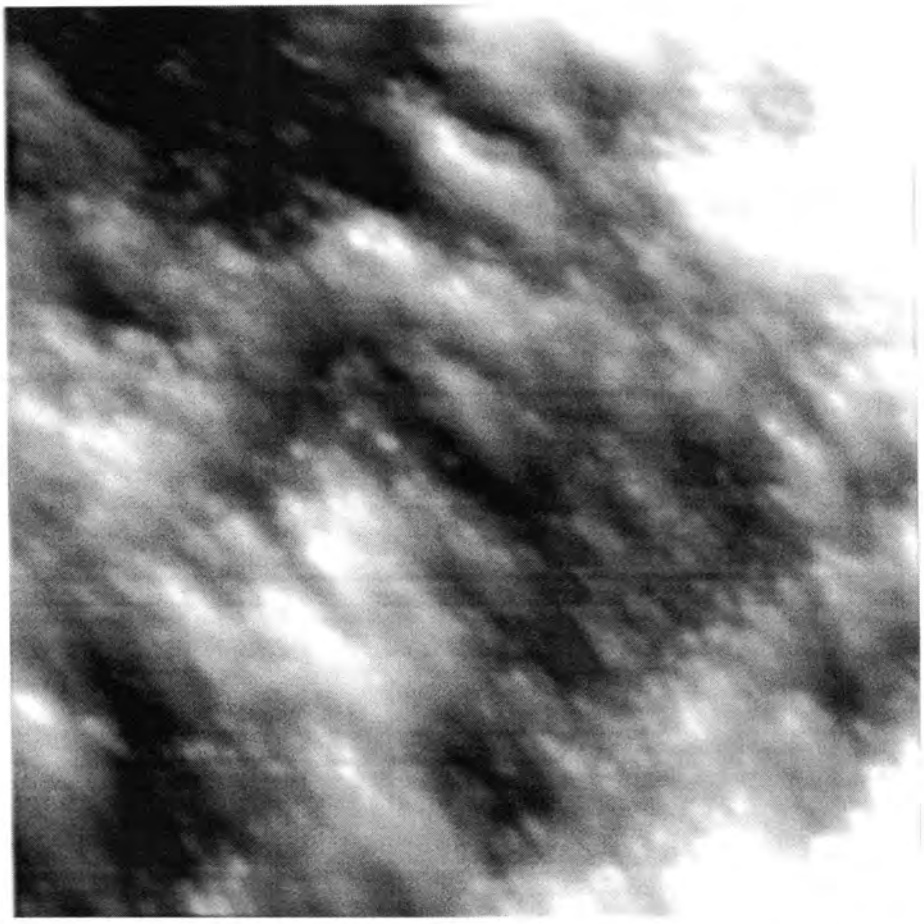

Figure 16: STM image obtained from Al-Ni-Co oriented to the $(0,\bar{1},\bar{1},0,1)$ plane.

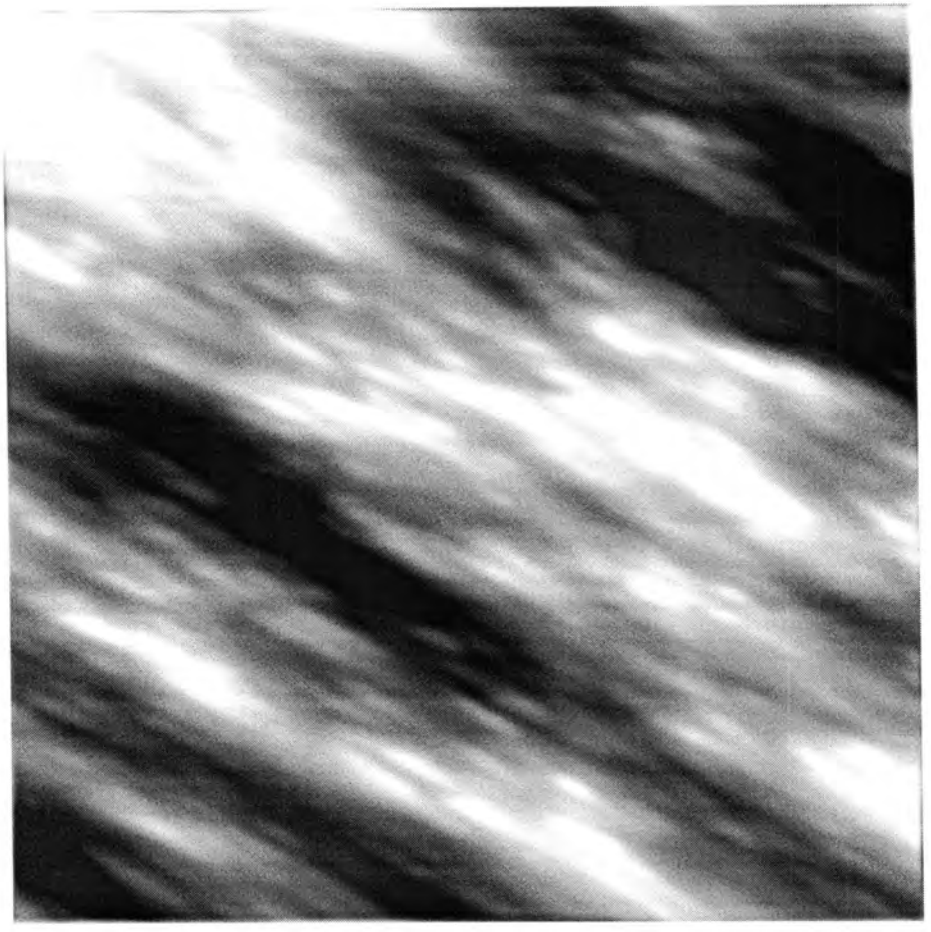

25 x 25 nm^2

Figure 17: STM image obtained from Al-Ni-Co oriented to the $(0,\bar{1},\bar{1},0,1)$ plane.

Figure 18: STM image obtained from Al-Ni-Co oriented to the $(0,\bar{1},\bar{1},0,1)$ plane.

An inspection of the STM images indicated that there were not any terraces or step edges typical of periodic crystals or the 10-fold surface. Instead, the images appeared to reveal a layered structure. This layering emerged regardless of the scan size or the annealing temperature. However, these images did seem to contain relatively flat areas separated by a sloped incline (see Figures 19 and 20). At first it was thought that the sloped incline could be the step edge, similar to the inclined step edges found on the 2-fold surface of Al-N-Co by Kishida et al.[12] In addition, the step heights predicted by Steurer contained sloped instead of sharp steps (see Figure 21), which also seemed to support the idea of inclined step edges for the net planes. Unfortunately, this conclusion is not borne out by the results. Steurer predicted step heights of 2.15 Å and 2.02 Å. The height differences in the STM images shown in Figures 20 and 21 were 0.32 Å, 1.81 Å, 1.10 Å, 2.36 Å, 1.31 Å, and 4.17 Å, which varied greatly from the predicted step heights.

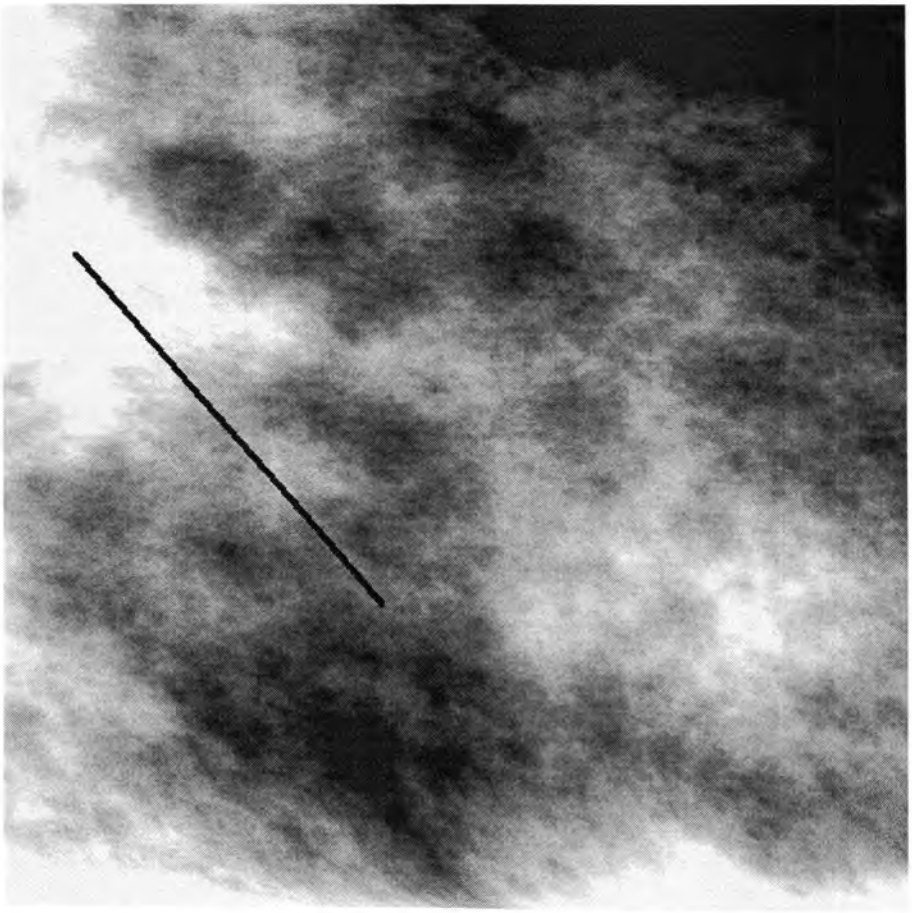

1000 x 1000 nm^2

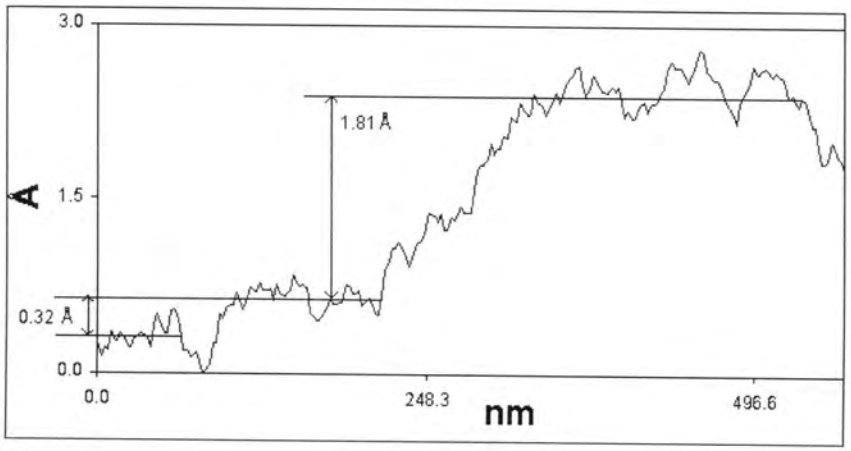

Figure 19: STM image obtained from Al-Ni-Co oriented to the $(0,\bar{1},\bar{1},0,1)$ plane and its corresponding line scan.

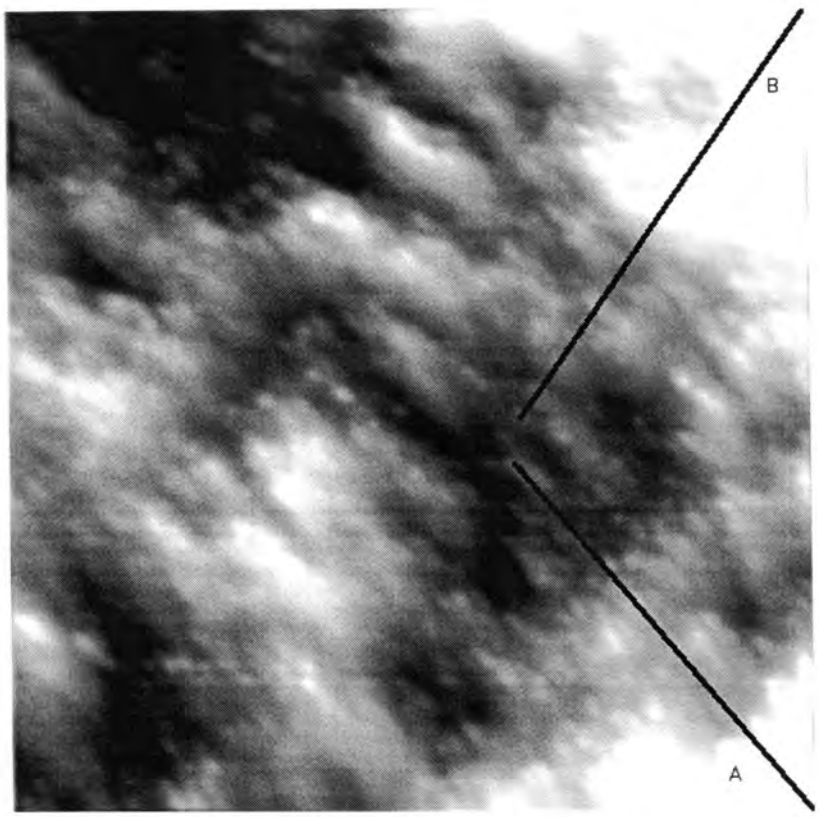

50 x 50 nm^2

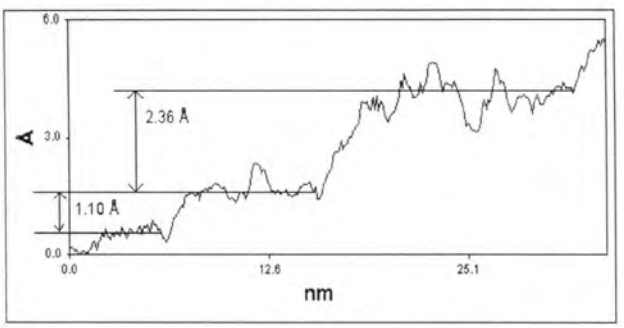

A

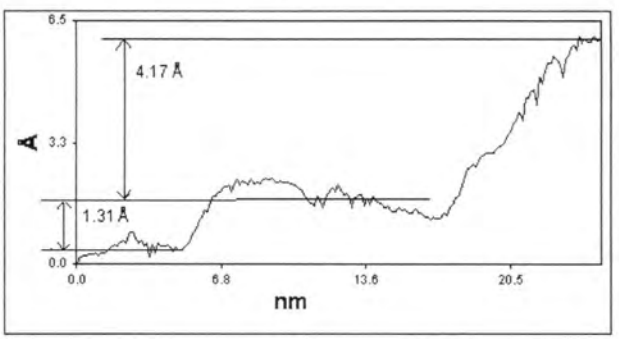

B

Figure 20: STM image obtained from Al-Ni-Co oriented to the $(0,\bar{1},\bar{1},0,1)$ plane and its corresponding line scans.

Figure 21: Predicted step heights for Al-Ni-Co oriented to the $(0,\bar{1},\bar{1},0,1)$ plane.

The FFT's of the STM images were also different than what is normally expected from a typical STM scan. These FFT's, rather than having a rotational symmetry axis, contain a center of inversion, as can be seen in Figure 22.

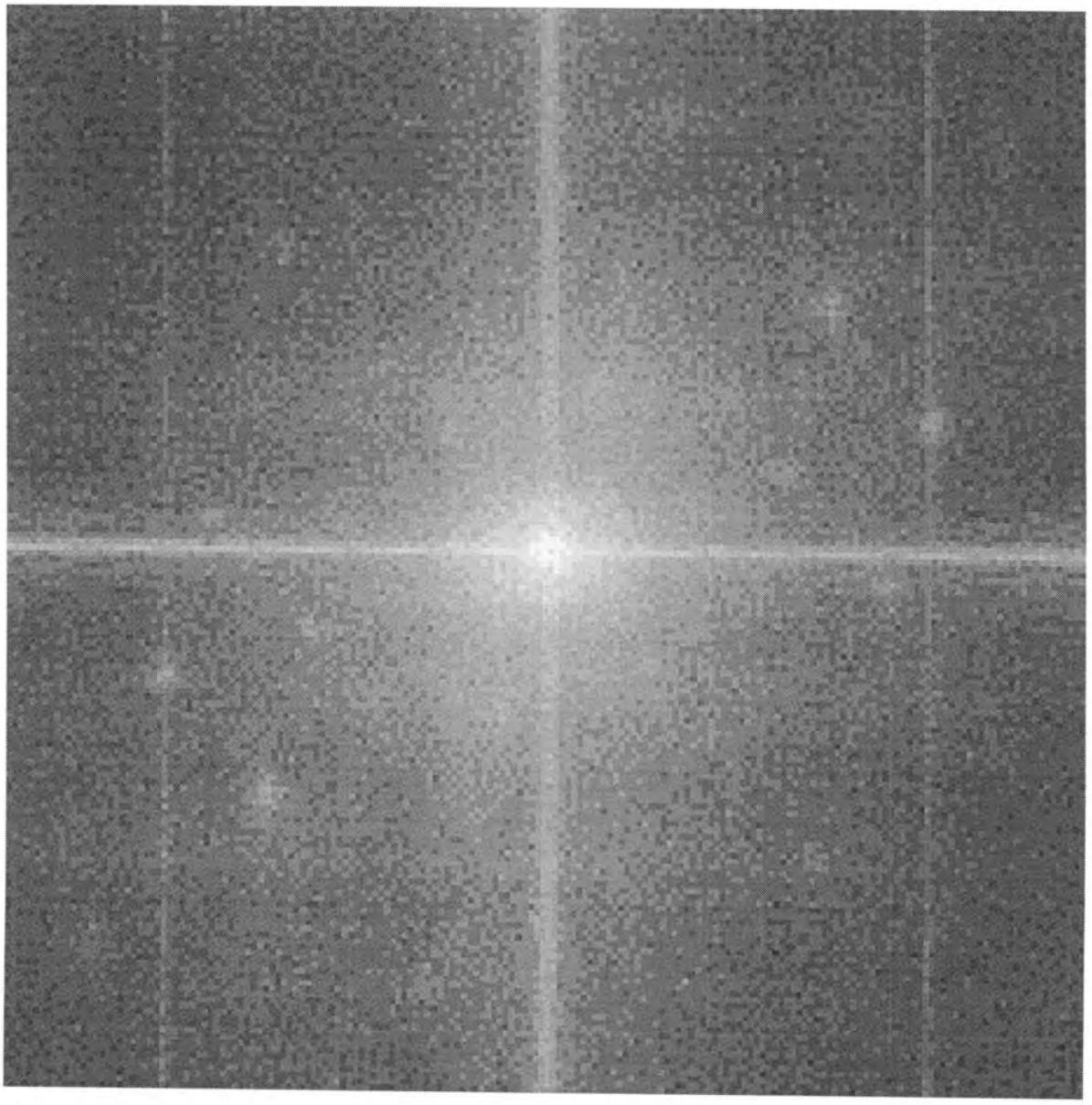

Figure 22: FFT of the 50 x 50 nm^2 STM image shown in Figure 17.

The most interesting observations made by STM are shown in Figures 23 and 24. These images indicate bumps on the surface. Although the scale of these images implies that the bumps are too large to be atoms, it is possible that they are clusters.

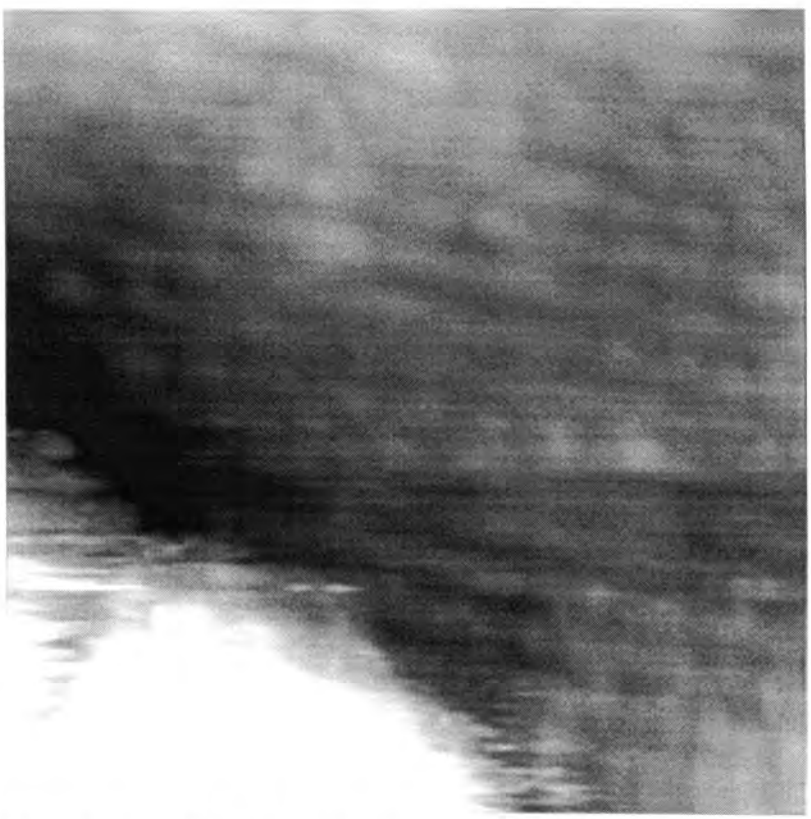

50 x 50 nm^2

Figure 23: STM image of Al-Ni-Co oriented to the $(0,\bar{1},\bar{1},0,1)$ plane.

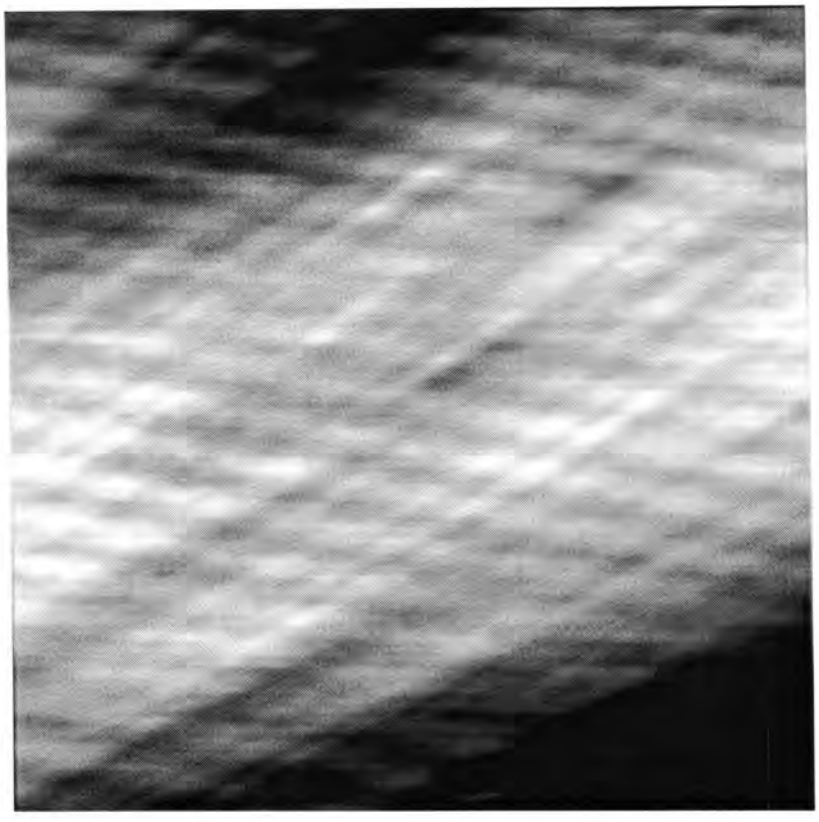

25 x 25 nm^2

Figure 24: STM image of Al-Ni-Co oriented to the $(0,\bar{1},\bar{1},0,1)$ plane.

The STM image pictured in Figure 24 is explored further in Figure 25 below. Line scans across the image in various directions reveal the spacing between the bumps. For the first line scan, labeled A in Figure 25, the spacing is 1.40 nm. For the second line scan, labeled B, the spacing is 1.88 nm. Finally, the third line scan, labeled C, reveals spacings of 1.83 nm and 1.43 nm. It is interesting to note that the ratio 1.83 nm/1.43 nm equals 1.28, which is approximately equal to the square root of the golden mean, $\tau^{1/2}$. Since $\tau = (1+\sqrt{5})/2 = 1.618$, $\tau^{1/2} = 1.27$. Thus, it appears that the spacing between the clusters may be related to the Fibonacci sequence.

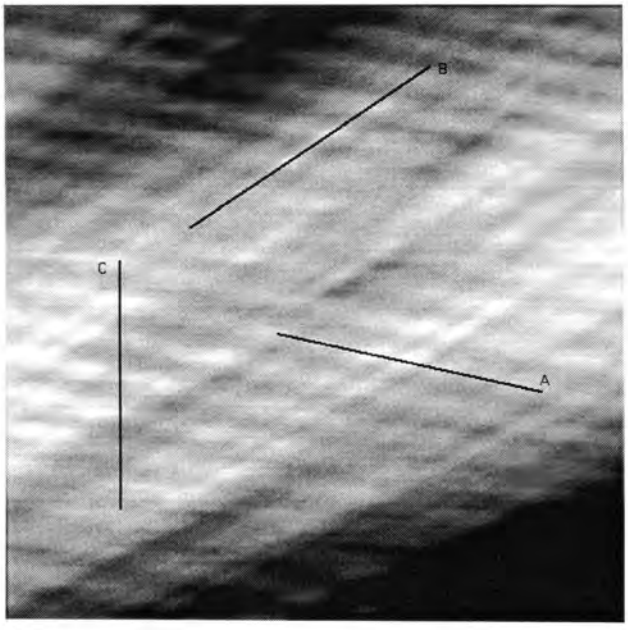

25 x 25 nm^2

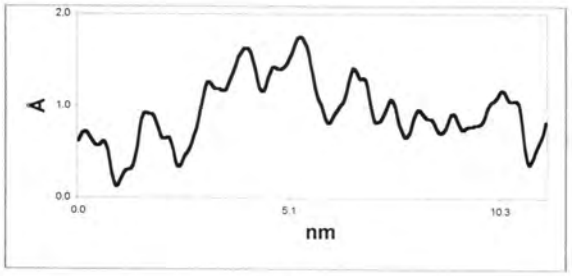

A

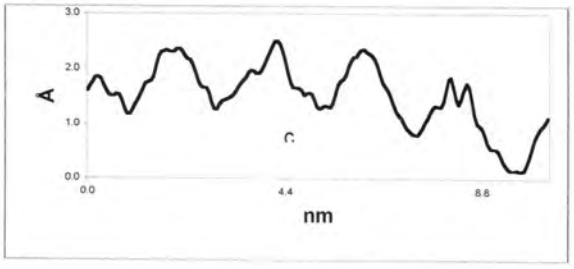

B

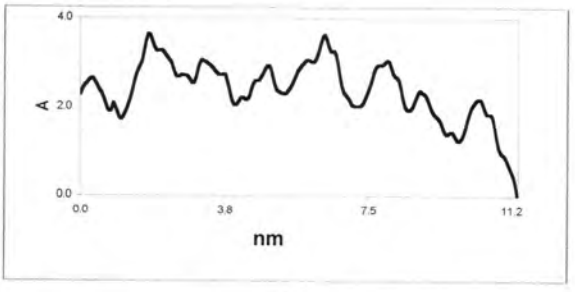

C

Figure 25: STM image shown in Figure 25 containing line scans in various directions.

Finally, a comparison of Figure 24 and Figure 10 was performed. It was expected that the real-space STM image shown in Figure 24 would be rotated 90 degrees from the reciprocal space LEED pattern portrayed in Figure 10. For convenience, both images are copied below in Figure 26. As expected, the LEED pattern does appear to be rotated by 90 degrees from the STM image. This observation indicates that the lined LEED patterns observed for all samples are stable images caused by the "clusters" within the quasicrystals.

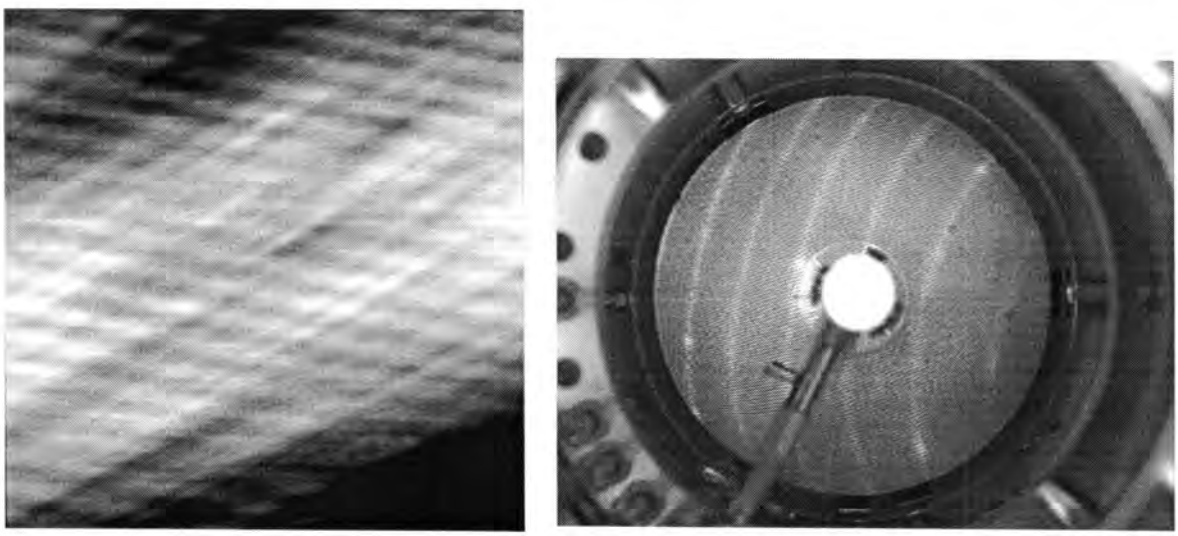

25 x 25 nm^2 91 eV

Figure 26: Comparison of the real-space STM image versus the reciprocal LEED image for Al-Ni-Co oriented to the $(0,\bar{1},\bar{1},0,1)$ plane.

CONCLUSION

The experiments discussed here have examined the question of whether net planes were stable terminations of the decagonal quasicrystal structure. This hypothesis was tested using LEED and STM experiments. If the net planes were stable terminations, the faceting of vicinal surfaces to the net planes would occur. This faceting would be indicated in LEED patterns. Additionally, stable net planes would have terrace-step structure that reflected the bulk structure. This consequence was examined using STM imaging.

The results indicated that stable planes linking the 10-fold and 2-fold axes in Al-Ni-Co do exist. This conclusion is supported by the LEED experiments conducted in the LEED chamber and the VT-STM chamber. Within the LEED chamber, two of the samples, ARR-2-137-1 and ARR-2-137-2, appeared to facet to the $(1,1,\bar{1},\bar{1},2)$ plane. In contrast, the third sample, ARR-2-102-2, which was oriented three degrees off the $(1,1,\bar{1},\bar{1},2)$ plane in the $[0,\bar{1},\bar{1},0,1]$ direction, faceted to the same plane as the VT-STM chamber sample, which was cut to the $(0,\bar{1},\bar{1},0,1)$ plane. Thus, the LEED patterns support the existence of stable net planes in decagonal quasicrystals.

In addition, the incline planes exhibited characteristics that differed from the 10-fold axis. Firstly, the LEED patterns obtained for all samples in both chambers were unique. All LEED patterns contained only one mirror plane and their intensities would diminish quickly with time, indicating that they were very sensitive to surface contamination. Secondly, all Al-Ni-Co samples cut to an inclined plane would

produce a lined LEED pattern, indicating that they are periodic in one direction while being disordered in another direction. Thirdly, the STM images obtained for the sample in the VT-STM chamber did not produce terraces or steps. Lastly, the STM images indicated that the net planes consist of "clusters" rather than atoms.

Finally, the experimental data obtained from the sample in the VT-STM chamber did not agree with Steurer's predictions. The LEED patterns produced by the sample did not adequately match the LEED pattern predictions, and thus it was concluded that they were not the same. Additionally, the STM images obtained did not seem to produce step heights that could be equivalent to Steurer's predicted step heights of 2.15 Å and 2.02 Å. Therefore, neither the LEED patterns nor the STM images supported the predictions for Al-Ni-Co oriented to the $(0,\overline{1},\overline{1},0,1)$ plane.

In conclusion, it is apparent that stable net planes do exist in decagonal Al-Ni-Co. These planes contain characteristics that make them unique from the 10-fold and 2-fold surfaces. However, the results obtained experimentally from decagonal Al-Ni-Co oriented to the $(0\overline{1}\,\overline{1}01)$ plane did not agree with predictions made by Steurer. Thus, it is apparent that more studies regarding the properties of net planes should be undertaken.

REFERENCES

1. Shechtman, D.; Lang, C. Quasiperiodic Materials: Discovery and Recent Developments. *MRS Bulletin* **November 1997,** *22*; 40-42.

2. Nelson, D. R. Quasicrystals. *Scientific American* **1986,** *259*, 43-51.

3. Stephens, P. W.; Goldman, A. I. The Structure of Quasicrystals. *Scientific American* **1991,** *264*, 24-31.

4. Ebert, P.; Chao, K.-J.; Niu, Q.; Shih, C. K. Dislocations, Phason Defects, and Domain Walls in a One-Dimensional Quasiperiodic Superstructure of a Metallic Thin Film. *Phys. Rev. Lett.* **1999,** *83*, 3222-3225.

5. Tsai, A. P.; Inoue, A.; Masumoto, T. Stable decagonal aluminum-cobalt-nickel and aluminum-cobalt-copper quasicrystals. *Materials Transactions, JIM* **1989,** *30*, 463-473.

6. Steurer, W.; Cervellino, A. Quasiperiodicity in decagonal phases forced by inclined net planes? *Acta Crystallographica* **2001,** *A57*, 333-340.

7. Janot, C. How to Fill Space with Atoms in Condensed Matter States. *Quasicrystals: A Primer*, 2nd Edition; Clarendon Press: Oxford, 1994; 22-52.

8. Steurer, W.; Haibach, T. The periodic average structure of particular quasicrystals. *Acta Crystallographica* **1999,** *A55*, 48-57.

9. McLean, J. G.; Kruse, P.; Kummel, A. C. Atomic Structure Determination for GaAs(001)-(6x6) by STM. *Surface Science* **1999,** *424*, 206-218.

10. Clarke, L. J. Applications of kinematic theory. *Surface Crystallography: An Introduction to Low Energy Electron Diffraction*; John Wiley and Sons: New York, 1985; 234-239.

11. Gerlach, R. L.; Rhodin, T. N. Structure Analysis of Alkali Metal Adsorption on Single Crystal Nickel Surfaces. *Surface Science* **1969,** *17*, 32-68.

12. Kishida, M.; Kamimura, Y.; Tamura, R.; Edagawa, K.; Takeuchi, S.; Sato, T.; Yokoyama, Y.; Guo, J. Q.; Tsai, A. P. Scanning Tunneling Microscopy of Al-Ni-Co Decagonal Quasicrystal. *Physical Review B: Condensed Matter and Material Physics* **2002,** *65*, 4208-4216.

13. Weber, S. Steffen Weber's Homepage. http://www.jcrystal.com/steffenweber/ (accessed July 18, 2002), http://www.jcrystal.com/steffenweber/JAVA/qcjlaue.html.

14. Takakure, H.; Yamamoto, A.; Tsai, A. P.; *Acta Crystallographica* .**2001,** *A57*, 567-585.

ACKNOWLEDGMENTS

First, I would like to thank my major professor, Dr. Patricia A. Thiel, for her patience and support during my time as a graduate student.

I am also grateful to Dr. Cynthia Jenks, who has worked closely with me on this project. She answered my many questions, struggled through instrumental problems with me, and provided a lot of advice and support throughout the time spent as a graduate student, for which I am very thankful.

I would like to thank all the members of the Thiel group for their advise and support, especially Dr. Tanhong Cai, who spent time explaining theories and answering my questions.

Finally, I would like to thank my family and friends, notably Andrea, Angie, Ben, Brad and Laura, for listening to the details and mishaps of my research project and providing advice and encouragement.

This work was performed at the Ames Laboratory and is supported by the U.S. Department of Energy, Office of Basic Energy Sciences, Division of Materials Sciences under contract No. W-405-Eng-82.

APPENDIX 1: The Average Periodic Structure of Quasicrystals

A characteristic of quasicrystals is that they do not exhibit periodicity in three-dimensional space. However, using oblique projections of particular crystal structures onto physical space, periodic average structures can be obtained.[8] To understand the construction of a periodic average structure, it is necessary to review the embedding of a quasiperiodic structure in a high-dimensional periodic space. This embedding for a one-dimensional quasicrystal can be described by two methods: the strip and projection method and the cut method.[7] Steurer employs the cut method when demonstrating the construction of periodic average structure of a one-dimensional quasicrystal (See Figure 27).

The cut method begins with a periodic two-dimensional square lattice. Here, the square lattice (d_1, d_2) is decorated by a set of segment lines of height Δ with a component only in the perpendicular direction $V^{\perp}$. These lines are often called "atomic surfaces" or hyperatoms. If a line of an irrational slope is cut through the lattice, the points at which parallel space $V^{||}$ intersects the atomic surfaces will produce a quasiperiodic sequence of long and short segments, L and S respectively, along parallel space. If the slope of the cut is equal to τ, the Fibonacci sequence is constructed.[6] The average structure of the Fibonacci sequence is then generated by oblique projection of the atomic surfaces onto parallel space. The oblique projection direction is conducted along the gray strips shown in Figure 27. Although there are an infinite number of oblique projections resulting in discrete average structures, the direction illustrated is the only direction yielding a one-to-one mapping of the quasiperiodic structure onto the periodic average structure. The thick horizontal line

segments labeled A shown on $V^{||}$ are the hyperatoms of the average structure obtained. Notice that the average structure is periodically spaced in physical space.[8]

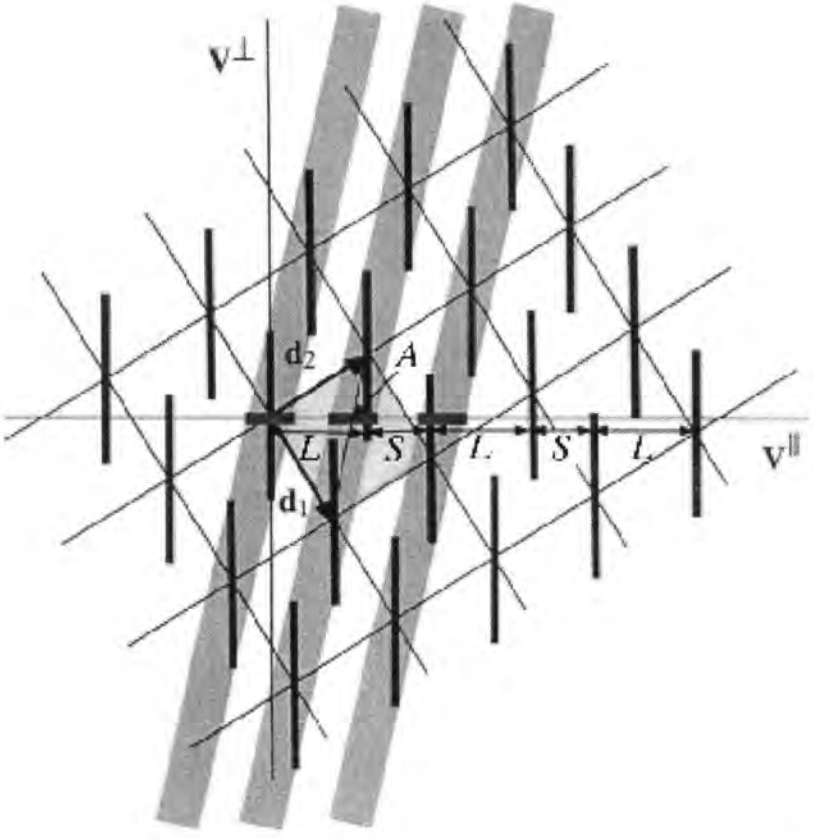

Figure 27: Illustration of constructing the periodic average structure of the Fibonacci sequence using the cut method.[8] *(used with permission)*

Likewise, average structures for two-dimensional quasicrystals, such as the Penrose tiling, can be constructed. The Penrose tiling can be constructed from an irrational cut of a four-dimensional hypercrystal structure with two-dimensional physical space (see Figure 28). The four-dimensional embedding space is composed of V_1, V_2, and V_3, which are the parallel space components and of V_4 and V_5, which are the perpendicular space components. The oblique projection direction used to obtain the periodic average structure is along the gray strip shown. The oblique projection causes the pentagonal atomic surfaces of the periodic structure to become distorted elliptically, as shown in Figure 29. In Figure 30, the resulting periodic average structure is superimposed on a Penrose tiling. Notice that the all the vertices of the Penrose tiling fall with the bounds of the atomic surfaces for the average structure and that the atomic surfaces are spaced periodically in two dimensions.[8]

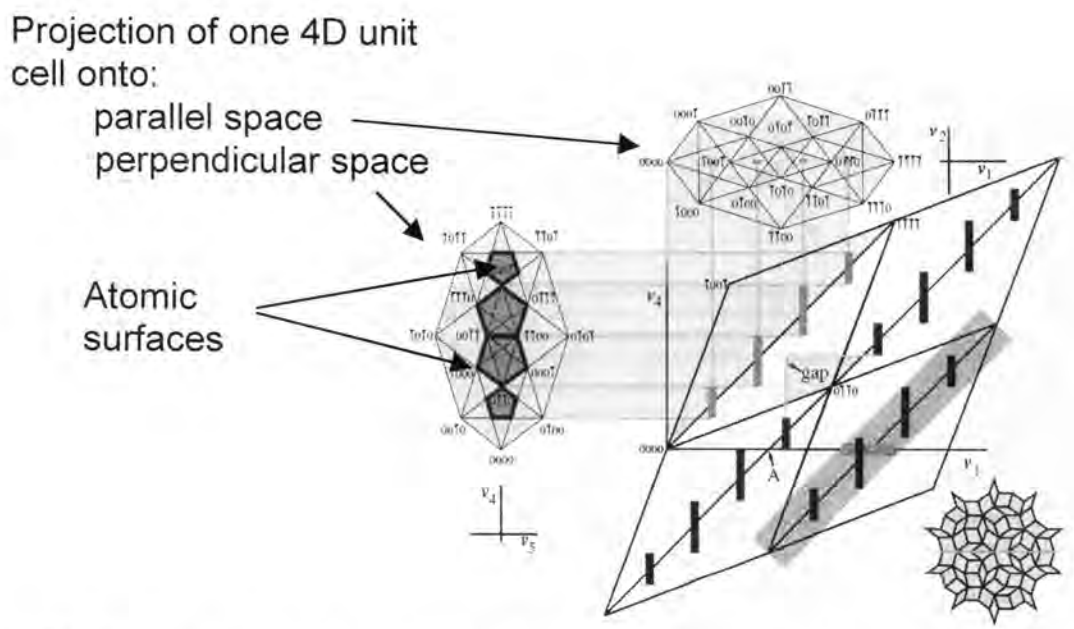

Figure 28: Illustration detailing the construction of a periodic average structure for the Penrose tiling.[8] *(used with permission)*

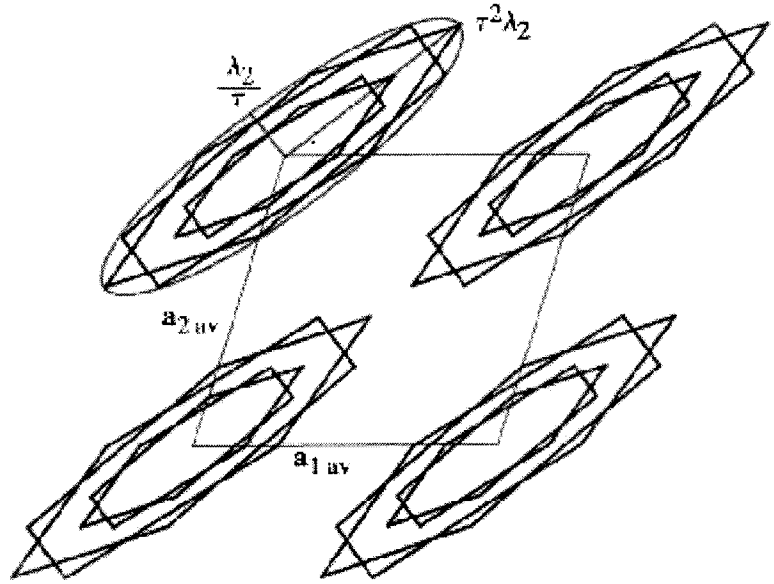

Figure 29: One unit cell of the average structure for the Penrose tiling decorated with the projected atomic surfaces.[8] *(used with permission)*

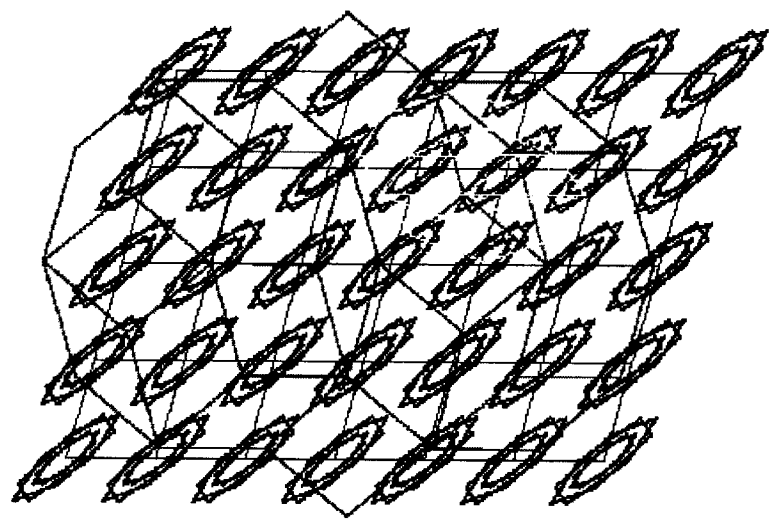

Figure 30: Projected periodic average structure superimposed onto a Penrose tiling.[8] *(used with permission)*

This concept of periodic average structures can be utilized in the case of the decagonal quasicrystal Al-Ni-Co. As mentioned previously, the quasiperiodic stacks inclined towards the 10-fold axis technically are not net planes because they are not inclusive of all the atoms. This is illustrated in the top parts of Figures 31a and 31b. Here, x_1, x_2, and x_3 represent physical (parallel) space components, while x_4, and x_5, represent complimentary (perpendicular) space. Additionally, x_3 is the 10-fold axis. Therefore, in the top parts of Figures 31a and 31b, the 10-fold axis is plotted versus a component of physical space. Thus, the dots shown are the positions of atoms in Al-Ni-Co. Next, some of the predicted net planes were drawn into the figures. As expected, not all of the atoms lie on the proposed net plane. To make the net planes inclusive of all the atoms in the structure, it is necessary to obtain the periodic average structure for Al-Ni-Co. Thus, the bottom parts of Figures 31a and 31b plot the 10-fold axis versus a component of perpendicular space. Accordingly, the oblique projections directions of two average periodic structures, AS-1 and AS-2, are detailed. The resulting periodic average structures for the projections shown in the bottom of Figures 31a and 31b are displayed in Figure 32 and Figure 33. Notice that all of the hyperatoms now lie on the predicted net planes.[6]

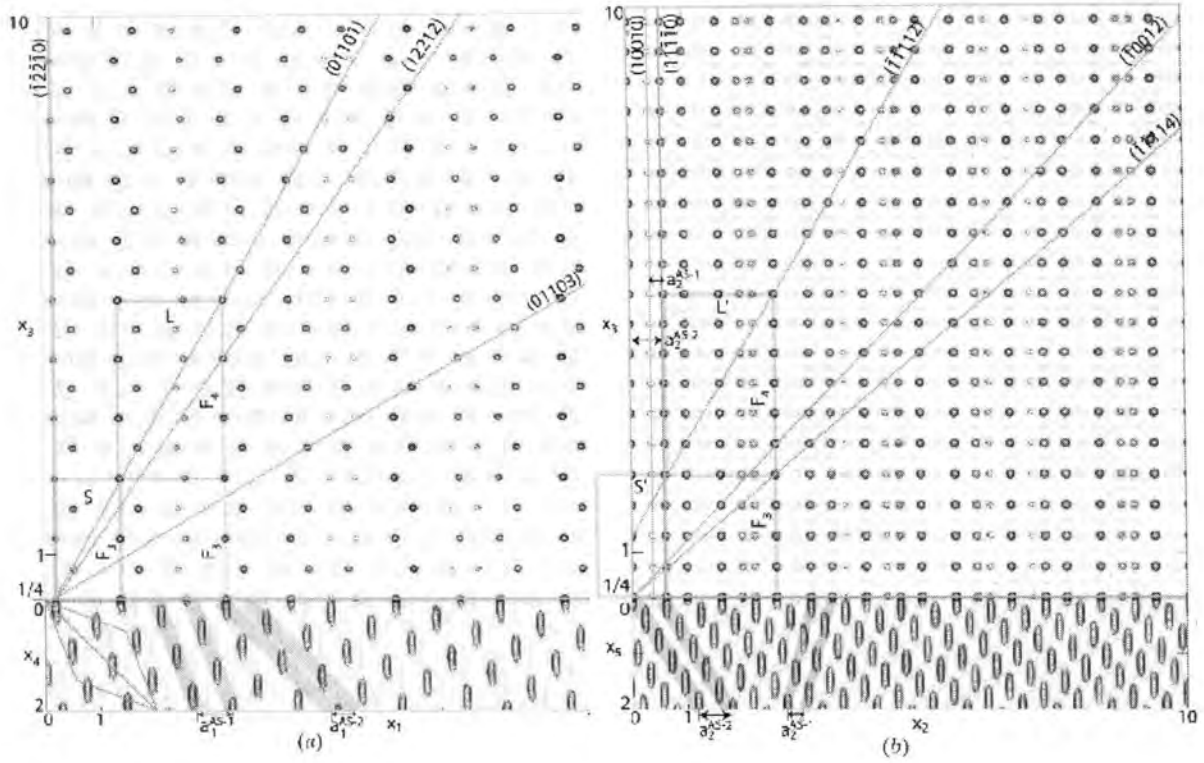

Figure 31: Structure of decagonal Al-Ni-Co projected onto (*a*) the (x_1, x_3) plane and (*b*) the (x_2, x_3) plane. Net planes perpendicular to these planes are shown. In the lower part of the figures illustrate the oblique projection directions utilized to obtain average structures AS-1 and AS-2.[6] *(used with permission)*

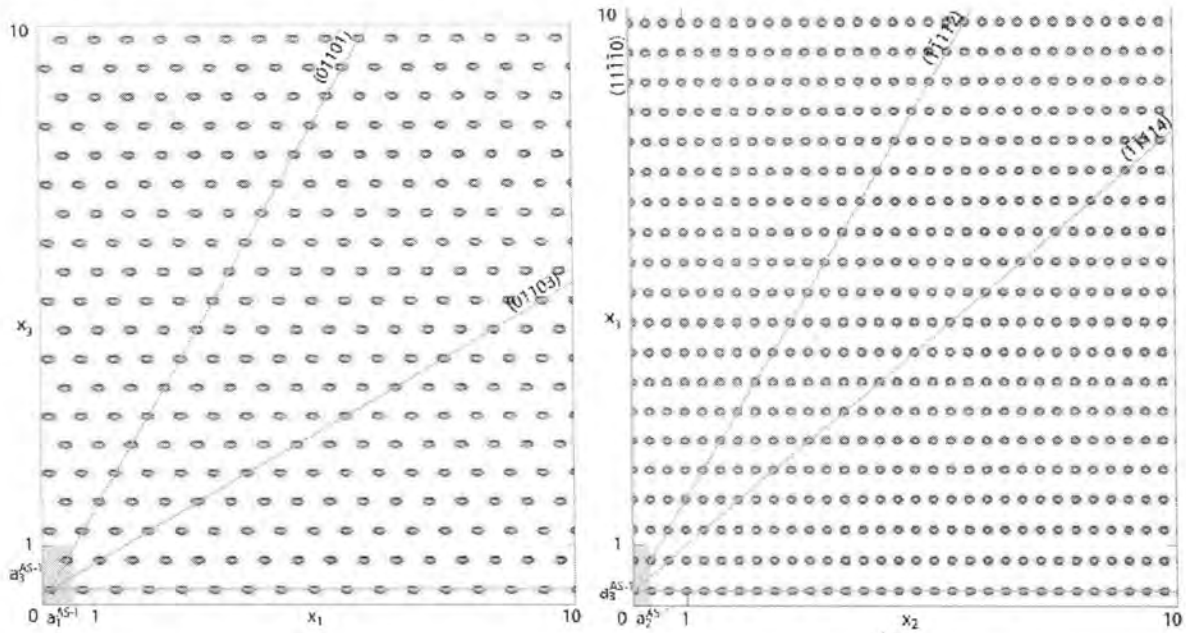

Figure 32: Average structure AS-1 for decagonal Al-Ni-Co projected onto (a) the (x_1, x_3) plane and (b) the (x_2, x_3) plane. Net planes perpendicular to these planes are shown.[6] *(used with permission)*

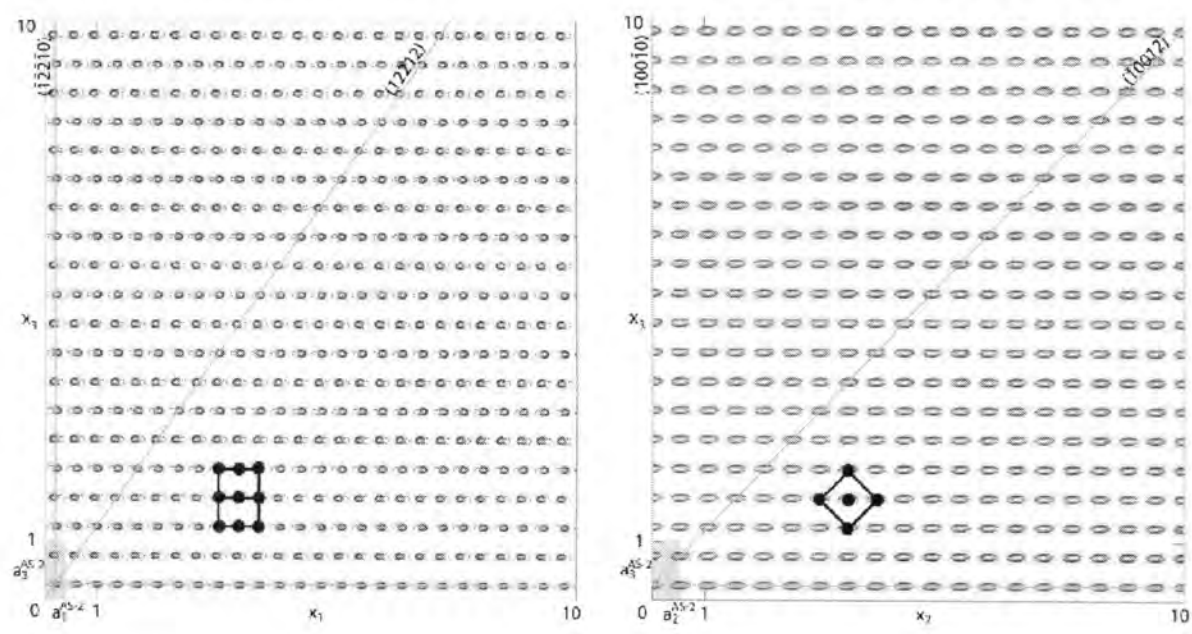

Figure 33: Average structure AS-2 for decagonal Al-Ni-Co projected onto (a) the (x_1, x_3) plane and (b) the (x_2, x_3) plane. Net planes perpendicular to these planes are shown.[6] *(used with permission)*

APPENDIX 2: Orienting Using Laue Patterns

Typically after cutting a sample, Laue patterns are used to precisely adjust the sample to the desired orientation. However, when trying to orient the Al-Ni-Co samples to the $(1,1,\bar{1},\bar{1},2)$ plane, the Laue patterns obtained were of very low intensity (see Figure 34).

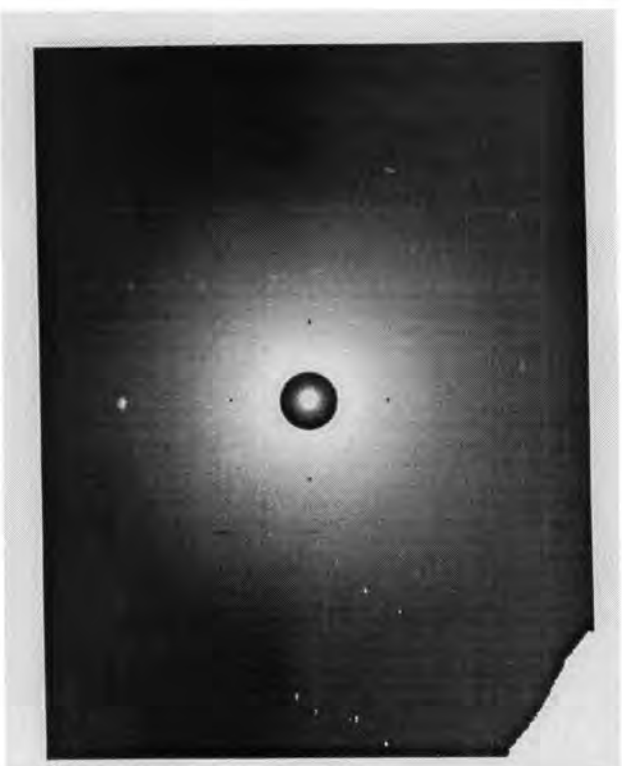

Figure 34: A Laue pattern obtained while trying to orient the Al-Ni-Co samples to the $(1,1,\bar{1},\bar{1},2)$ plane.

The lack of intensity led to a comparison between a computer-generated Laue pattern of Al-Ni-Co oriented to the $(1,1,\bar{1},\bar{1},2)$ plane (see Figure 35) to the experimentally obtained Laue patterns. A comparison of Figures 34 and 35 revealed that the Laue patterns were the same.

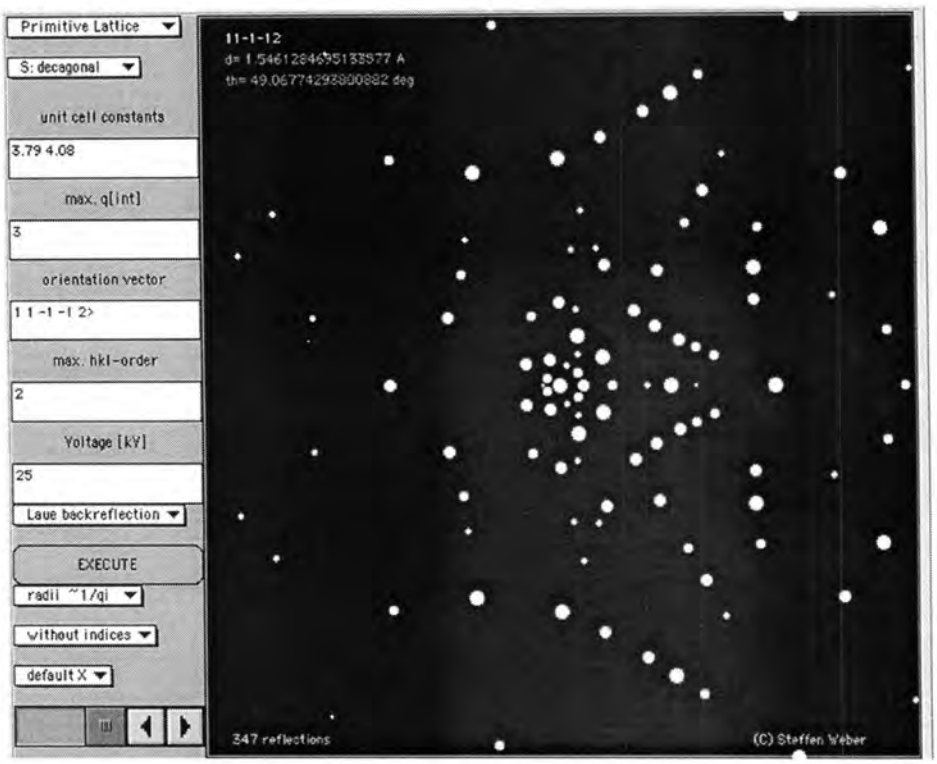

Figure 35: Predicted Laue pattern for decagonal Al-Ni-Co oriented to the $(1,1,\bar{1},\bar{1},2)$ plane.[13]

In order to precisely orient the samples, a horizontal and a vertical mirror plane are needed. As can be seen in Figure 35, the Laue patterns only contained a horizontal mirror plane. The question then arose on how to vertically orient the samples. It was discovered that if a line were drawn between two spots, one above and one below the center, it would pass through the center. These two spots are highlighted in Figure 36. Thus, these two spots were used to vertically orient the samples around $(1,1,\bar{1},\bar{1},2)$ plane.

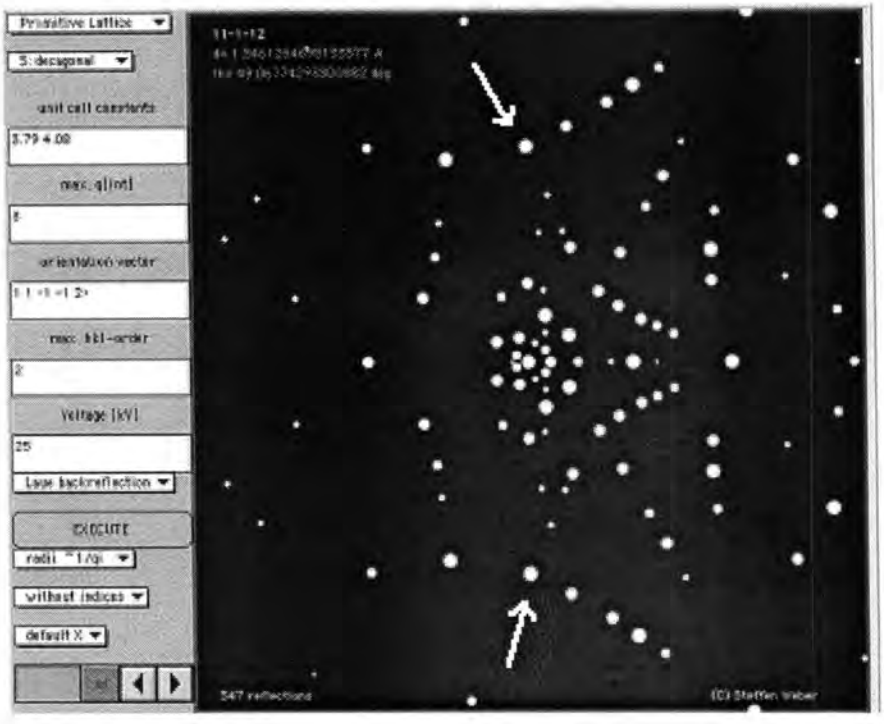

Figure 36: Predicted Laue pattern for decagonal Al-Ni-Co oriented to the $(1,1,\bar{1},\bar{1},2)$ plane.[13] The arrows are pointing to the two spots used to vertically orient the samples.

Sample ARR-2-102-2 was vertically oriented to the two dots highlighted in Figure 36. Sample ARR-2-137-2 was vertically oriented to the two dots to the right of those highlighted in Figure 36. These alignments are illustrated in Figure 37. Sample ARR-2-137-1 was oriented between the other two samples. However, the orientation of the samples remained difficult. The lack of intensity in the experimentally obtained Laue patterns made it difficult to recognize the desired spots for the vertical alignment.

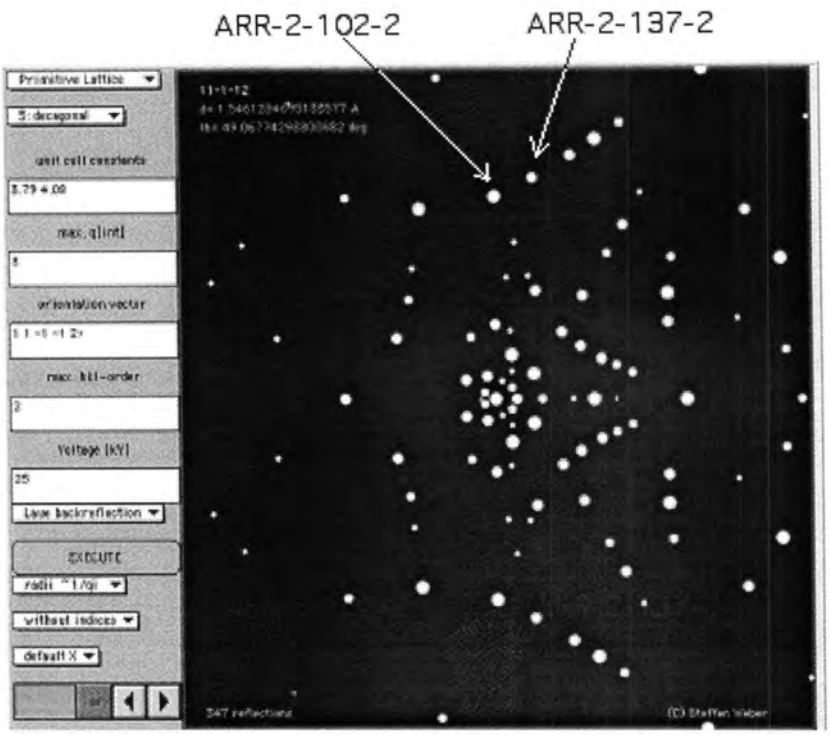

Figure 37: Predicted Laue pattern[13] illustrating where the vertical lines used to orient the decagonal Al-Ni-Co samples around the $(1,1,\overline{1},\overline{1},2)$ plane were located.

APPENDIX 3: LEED Lines

The LEED Chamber

As previously mentioned, LEED patterns containing lines rather than spots were found for all three samples in the LEED chamber (see Figure 7). The LEED patterns containing lines appeared to be as stable as those containing spots, if not more so. For example, the LEED patterns containing lines were first discovered after annealing at 900 K. However, no spots could be found in the LEED patterns after annealing at this temperature. Only after increasing the annealing temperature to 1100 K were the spots clearly visible. The lines, instead of disappearing with the increased annealing temperature, actually grew more intense. The result was that both the types of LEED patterns were obtainable. To switch between the two types, the position of the sample in front of the LEED optics was varied.

All of the lined LEED patterns contained three common characteristics. First, the lines were not consistent across the image. The lines towards the left of the image are straighter, while the lines towards the right of the image possessed more curvature. Second, when the beam energy was increased, the lines would move to the left. As a result, the spacing between the lines decreased as the beam energy increased. This characteristic is illustrated in Figure 38 below. Finally, upon close examination, there appear to be diffraction spots of higher intensity along the lines. These diffraction spots seem to correspond to the more prominent spots featured in the spotted LEED patterns. Specifically, this means that at first the LEED pattern contained lines, but as the sample was gradually moved horizontally in front of the

LEED optics, the lines faded away and the spots emerged. This correspondence is detailed in Figure 39.

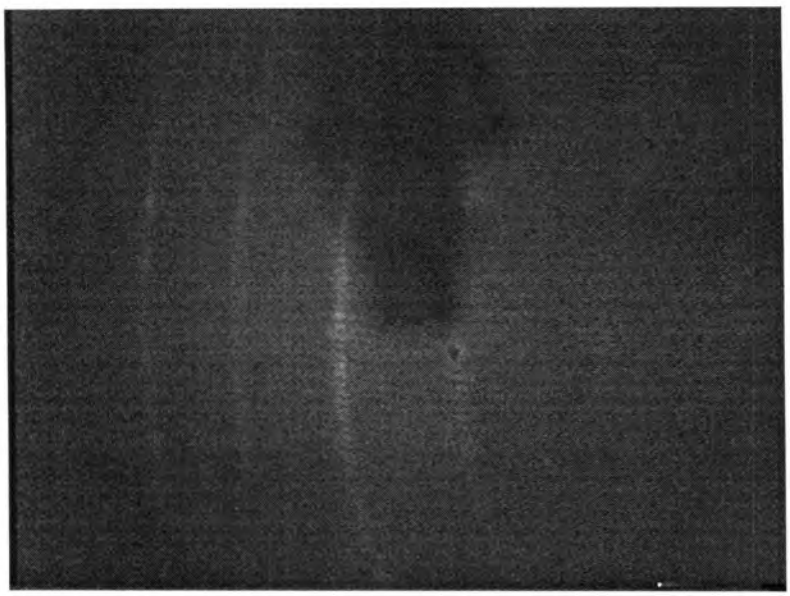

Low beam energy

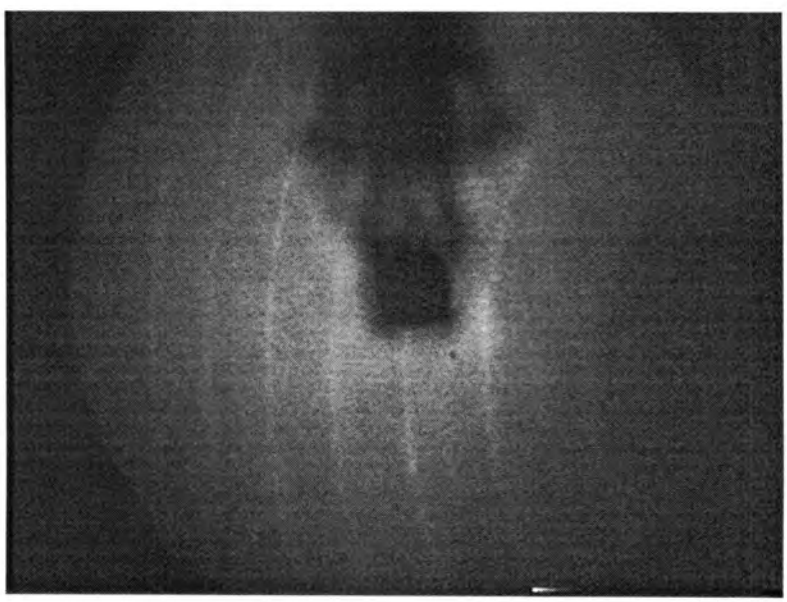

High beam energy

Figure 38: LEED patterns of Al-Ni-Co oriented around the $(1,1,\bar{1},\bar{1},2)$ plane at different beam energies.

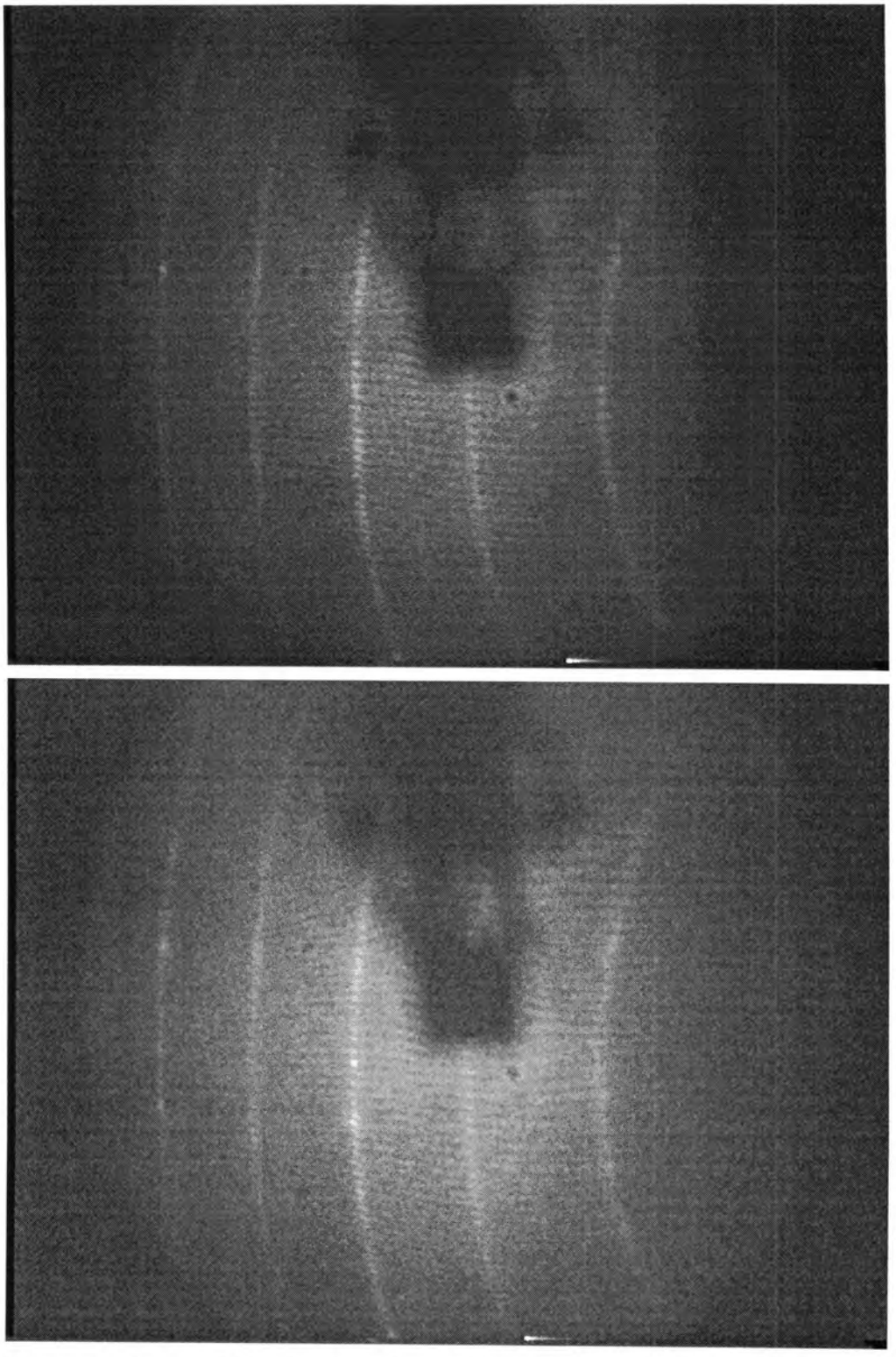

Figure 39: LEED patterns of Al-Ni-Co oriented around the $(1,1,\bar{1},\bar{1},2)$ plane. As the sample moved horizontally in front of the LEED optics at constant beam energy, a correlation between the lines and the spots could be observed.

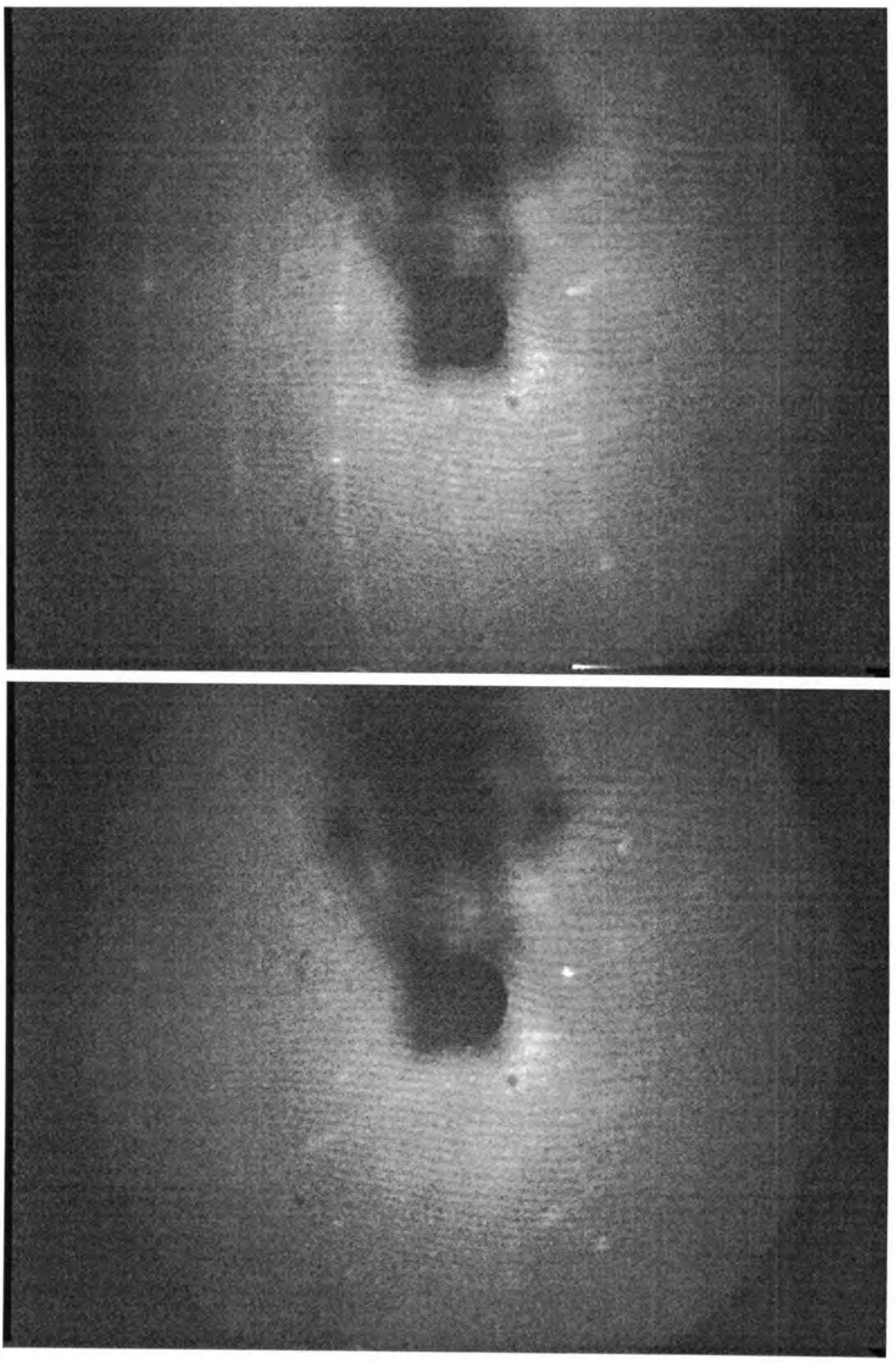

Figure 39: (continued).

The VT-STM Chamber

As with the $(1,1,\bar{1},\bar{1},2)$ surfaces, the sample oriented to the $(0,\bar{1},\bar{1},0,1)$ plane produce LEED images containing lines instead of spots. Similarly, these LEED patterns were obtained by varying the position of the sample in front of the LEED optics (see Figure 11). Like the lined LEED patterns that appeared for the Al-Ni-Co samples oriented to the $(1,1,\bar{1},\bar{1},2)$ plane, these patterns moved towards the left as the beam energy was increased. Additionally, the spacing between the lines decreased as the beam energy increased. Lastly, these LEED patterns contained diffraction spots of higher intensity that seemed to correspond with the spots in the spotted LEED pattern appearing at the same beam energy.

A qualitative comparison to bulk structure data was used to understand the spots of higher intensity found along the lined LEED patterns. This is a qualitative comparison because structural coordinates are not available for the large single crystal composition of $Al_{73}Ni_{10}Co_{17}$ used here. However, structure coordinates are available for $Al_{72}Ni_{20}Co_8$. $Al_{73}Ni_{10}Co_{17}$ tends to form a superstructure of the $Al_{72}Ni_{20}Co_8$ structure; therefore, this comparison is not unreasonable. Using the structure data of Takakura et al[14] for $Al_{72}Ni_{20}Co_8$, eight atomic layers were built and rotated so that the $(0,\bar{1},\bar{1},0,1)$ plane was exposed. As can be seen below in Figure 40, the bulk model predicts the lines observed in the LEED pattern from Figure 10. When one or two layers were exposed, the atoms aligned periodically in one direction and appeared to be disordered in the other direction. By taking the Fourier transform of the single model layer in Figure 40a, faint lines appear. As the number

of exposed layers was increased, the spots of high intensity would appear along the lines, as shown in Figure 40b. Therefore the diffraction lines are caused by periodic spacing, while the spots are due to atoms arranged in an orderly, albeit aperiodic, manner. Thus, when only spotted LEED patterns were observed, the region of the sample being observed must not have the aperiodic order arranged periodically.

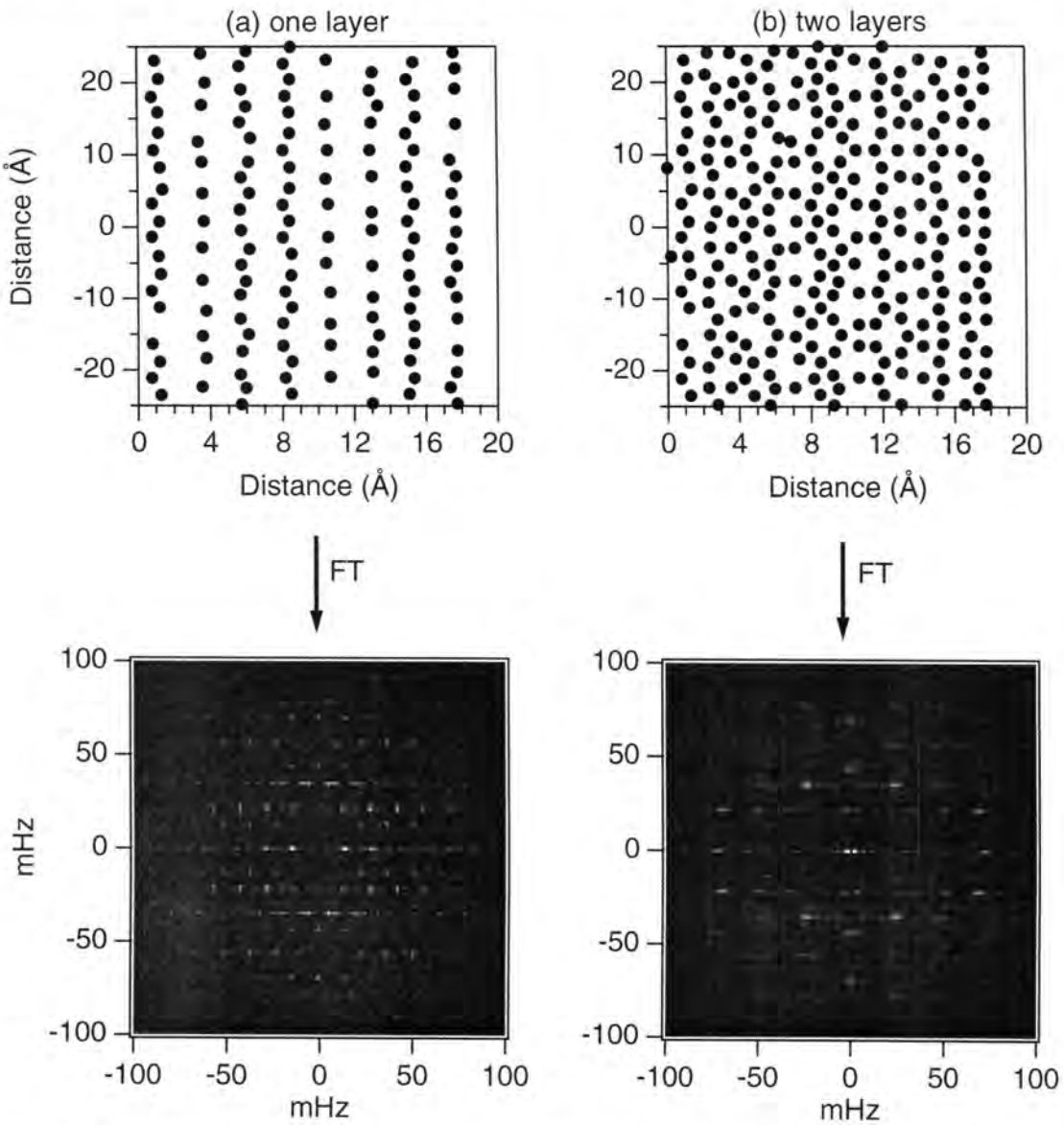

Figure 40: Results of calculations using bulk coordinates for (a) one layer of the surface of decagonal Al-Ni-Co oriented to the $(0,\bar{1},\bar{1},0,1)$ plane and its corresponding Fourier transform and for (b) two layers and its corresponding Fourier transform.

APPENDIX 4: LEED Comparison

It was necessary to compare the experimentally obtained LEED patterns for the Al-Ni-Co sample oriented to the $(0,\bar{1},\bar{1},0,1)$ plane (see Figure 8) to those predicted by Steurer (see Figure 9). Thus, an obvious difference between the predicted and experimental LEED patterns was discovered. The predicted LEED patterns contain both a horizontal mirror plane and a vertical mirror plane, while the experimental LEED patterns contain only a horizontal mirror plane. This difference may have been caused by the calculation used to produce the predicted LEED patterns. If the calculation introduced a center of inversion, the additional mirror plane would result.

To compare the experimental LEED patterns to the predicted LEED patterns, a vertical mirror plane needed to be inserted into the experimental LEED patterns. This process will be explained for the image appearing at 40 eV, which was the experimental LEED pattern most closely resembling the predicted LEED patterns. First, the most intense LEED spots were traced onto an overlaying piece of paper. Then, these traced spots were passed through the center of the image, creating a center of inversion. Thus, the LEED pattern now contained a horizontal and a vertical mirror plane. The resulting LEED image is shown in Figure 41.

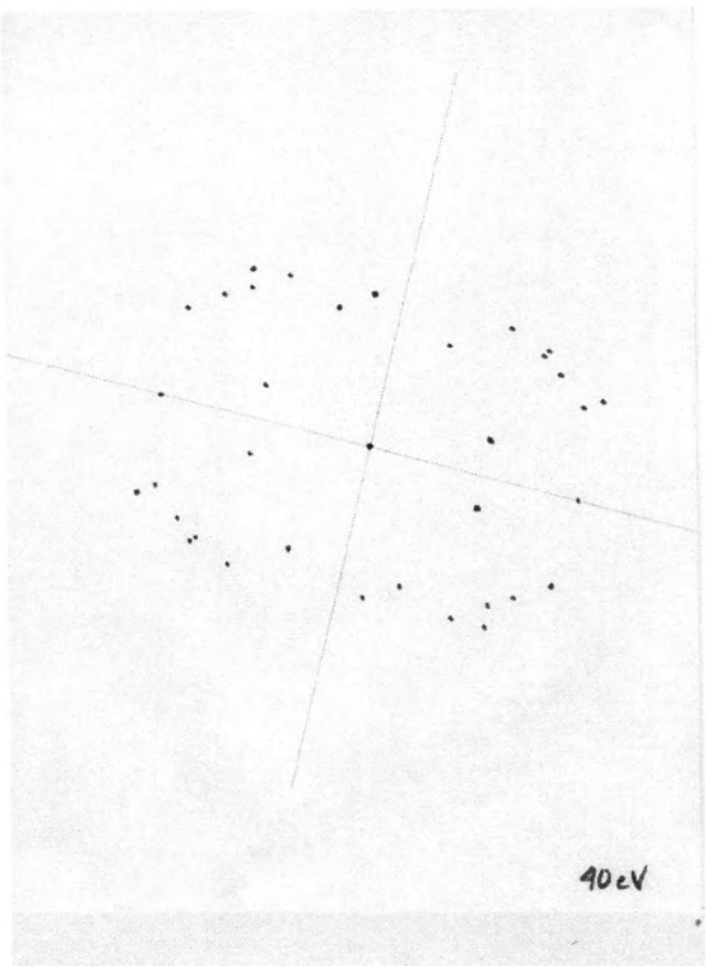

Figure 41: Experimental LEED pattern obtained for Al-Ni-Co oriented to the $(0,\bar{1},\bar{1},0,1)$ plane with an added center of inversion.

To aid the comparison between the experimental and the predicted LEED patterns, it was necessary to widen the images shown in Figure 9. First, the height-to-width ratio of the rectangle formed by the four innermost spots in Figure 41 was calculated. Then, the images in Figure 9 were widened until the height-to-width ratios for their corresponding rectangles equaled the ratio calculated from Figure 41. The result is shown below in Figure 42.

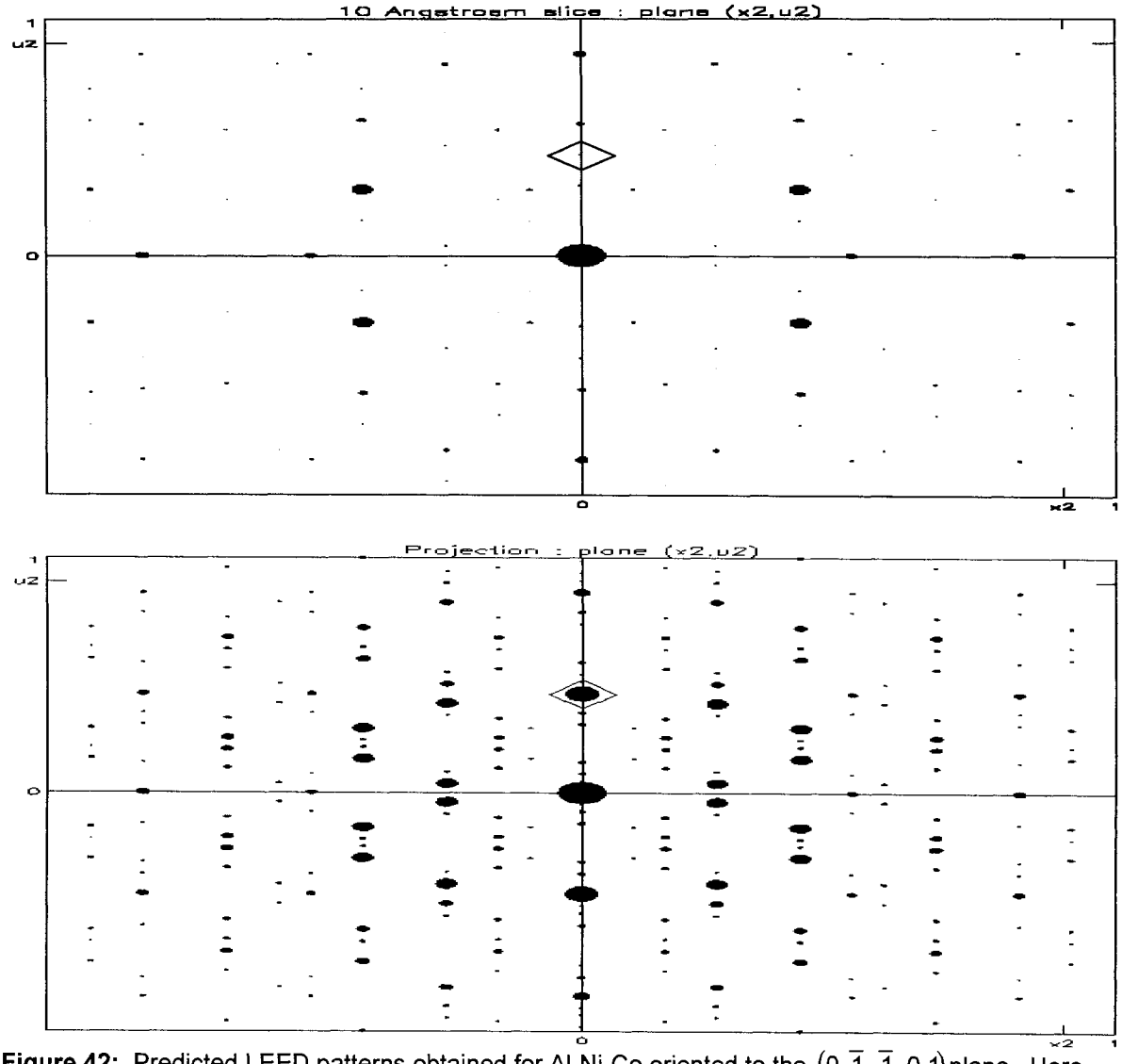

Figure 42: Predicted LEED patterns obtained for Al-Ni-Co oriented to the $(0,\bar{1},\bar{1},0,1)$ plane. Here the images are widened to produce the same vertical/horizontal ratio as the image shown in Figure 41.

When Figure 41 is compared to the images in Figure 42, there are some similarities. However, upon close examination the following inconsistencies were revealed. First, in order to show a relationship between Figures 41 and 42, spots with very small intensities must be employed in the two images from Figure 42. Using these spots counters the logic that the more intense spots in the predicted LEED patterns would be more likely to appear in the experimental LEED pattern. Second, there is not a satisfactory match in the alignment of the spots relative to each other. Finally, when doublets appear in Figure 41, they are aligned diagonally. According to both images in Figure 42, if doublets were to occur, they would be aligned vertically. Thus, it was concluded that the images were not the same.